Cutaneous barrier leakage and gut inflammation drive skin disease in Omenn syndrome

Rosita Rigoni, PhD,[a,b]* Elena Fontana, PhD,[b]* Kerry Dobbs, BS,[c] Veronica Marrella, PhD,[a,b] Valentina Taverniti, PhD,[d] Virginia Maina, PhD,[a,b] Amanda Facoetti, BS,[b,e] Giovanna D'Amico, PhD,[f] Waleed Al-Herz, MD,[g,h] Mario Ernesto Cruz-Munoz, PhD,[i] Catharina Schuetz, MD,[j] Andrew R. Gennery, MD,[k,l] Elizabeth K. Garabedian, RN, MSLS,[m] Silvia Giliani, PhD,[n,o] Deborah Draper, RN,[c] Ghassan Dbaibo, MD,[p] Raif S. Geha, MD,[q] Isabelle Meyts, MD, PhD,[r,s] Thomas Tousseyn, MD, PhD,[t] Benedicte Neven, PhD,[u,v] Despina Moshous, MD,[u,v] Alain Fischer, MD,[u,v] Ansgar Schulz, MD,[w] Andrea Finocchi, MD,[x] Douglas B. Kuhns, PhD,[y] Danielle L. Fink, MS,[y] Michail S. Lionakis, MD, ScD,[z] Muthulekha Swamydas, PhD,[z] Simone Guglielmetti, PhD,[d] Julie Alejo, BS,[aa] Ian A. Myles, MD, MPH,[c] Stefania Pittaluga, MD, PhD,[aa] Luigi D. Notarangelo, MD,[c] Anna Villa, MD,[a,bb] and Barbara Cassani, PhD[a,b]‡

Milan, Monza, Brescia, and Rome, Italy; Bethesda and Frederick, Md; Kuwait City, Kuwait; Cuernavaca, Mexico; Dresden and Ulm, Germany; Newcastle upon Tyne, United Kingdom; Beirut, Lebanon; Boston, Mass; Leuven, Belgium; and Paris, France

Background: Severe early-onset erythroderma and gut inflammation, with massive tissue infiltration of oligoclonal activated T cells are the hallmark of Omenn syndrome (OS).

Objective: The impact of altered gut homeostasis in the cutaneous manifestations of OS remains to be clarified.

Methods: We analyzed a cohort of 15 patients with OS and the 129Sv/C57BL/6 knock-in *Rag2*$^{R229Q/R229Q}$ (*Rag2*^{R229Q}) mouse model. Homing phenotypes of circulating lymphocytes were analyzed by flow cytometry. Inflammatory cytokines and chemokines were examined in the sera by ELISA and in skin biopsies by immunohistochemistry and *in situ* RNA hybridization. Experimental colitis was induced in mice by dextran sulfate sodium salt.

Results: We show that memory/activated T cells from patients with OS and from the *Rag2*^{R229Q} mouse model of OS abundantly express the skin homing receptors cutaneous lymphocyte associated antigen and CCR4 (Ccr4), associated with high levels of chemokine C-C motif ligands 17 and 22. Serum levels of LPS are also elevated. A broad $T_H1/T_H2/T_H17$ inflammatory signature is detected in the periphery and in the skin. Increased *Tlr4* expression in the skin of *Rag2*^{R229Q} mice is associated with enhanced cutaneous inflammation on local and systemic administration of LPS. Likewise, boosting colitis in *Rag2*^{R229Q} mice results in increased frequency of Ccr4$^+$ splenic T cells and worsening of skin inflammation, as indicated by epidermal thickening, enhanced epithelial cell activation, and dermal infiltration by T_H1 effector T cells.

From [a]the Milan Unit, Institute for Genetic and Biomedical Research (IRGB) National Research Council (CNR); [b]the Humanitas Clinical and Research Center IRCCS, Rozzano, Milan; [c]the Laboratory of Clinical Immunology and Microbiology, National Institute of Allergy and Infectious Diseases, National Institutes of Health (NIH), Bethesda; [d]the Department of Food, Environmental, and Nutritional Sciences, University of Milan; [e]the Humanitas University, Rozzano, Milan; [f]the Centro Ricerca Tettamanti, Clinica Pediatrica, Università Milano-Bicocca, Monza; [g]the Department of Pediatrics, Faculty of Medicine, Kuwait University; [h]the Allergy and Clinical Immunology Unit, Pediatric Department, Al-Sabah Hospital, Kuwait City; [i]the Facultad de Medicina, Universidad Autónoma del Estado de Morelos, Cuernavaca; [j]the Department of Pediatrics, Medizinische Fakultät Carl Gustav Carus, Technische Universität Dresden; [k]the Great North Children's Hospital, Clinical Resource Building, Newcastle upon Tyne; [l]the Institute of Cellular Medicine, Newcastle University; [m]the National Human Genome Research Institute, NIH, Bethesda; [n]the Department of Molecular and Translational Medicine, University of Brescia; [o]the Cytogenetic and Medical Genetics Unit, "A. Nocivelli" Institute for Molecular Medicine, Spedali Civili Hospital, Brescia; [p]the Department of Pediatrics and Adolescent Medicine, American University of Beirut Medical Center; [q]the Division of Immunology, Boston Children's Hospital, Harvard Medical School; [r]the Department of Pediatrics, Universitair Ziekenhuis Leuven, University Hospitals Leuven; [s]the Laboratory for Inborn Errors of Immunity, Department of Immunology, Microbiology and Transplantation, and [t]the Lab for Translational Cell and Tissue Research, Department of Imaging and Pathology, Katholieke Universiteit Leuven; [u]the Imagine Institute, Paris Descartes–Sorbonne Paris Cité University; [v]the Pediatric Immuno-Hematology Unit, Necker Children Hospital, Assistance Publique–Hôpitaux de Paris; [w]the Department of Pediatrics and Adolescent Medicine, University Medical Center Ulm; [x]the Department of Pediatrics, Children's Hospital Bambino Gesù, Rome; [y]the Neutrophil Monitoring Laboratory, Leidos Biomedical Research, Inc, Frederick National Laboratory for Cancer Research; [z]the Fungal Pathogenesis Section, Laboratory of Clinical Immunology and Microbiology, National Institute of Allergy and Infectious Diseases, and [aa]the Laboratory of Pathology, Center for Cancer Research, National Cancer Institute, NIH, Bethesda; and [bb]the Telethon Institute for Gene Therapy, Division of Regenerative Medicine, Stem Cells, and Gene Therapy, IRCCS San Raffaele Scientific Institute, Milan.

*These authors contributed equally.

‡Lead contact.

This work was partially supported by grants from the Italian Ministry of Health (GR-2011-02349759 to B. Cassani; PE-2016_02363691 to A. Villa, E. Fontana, and L.D. Notarangelo) and the Italian Fondazione Telethon (TIGET E2 Core grant). L.D. Notarangelo is supported by the Division of Intramural Research, National Institute of Allergy and Infectious Diseases, National Institutes of Health.

Disclosure of potential conflict of interest: The authors declare that they have no relevant conflicts of interest.

Received for publication September 18, 2019; revised March 11, 2020; accepted for publication April 6, 2020.

Corresponding authors: Barbara Cassani, PhD, Milan Unit, Institute for Genetic and Biomedical Research (IRGB) National Research Council (CNR), via Manzoni 113, 20089 Rozzano, Milan, Italy. E-mail: barbara.cassani@humanitasresearch.it. Or: Anna Villa, MD, San Raffaele Telethon Institute for Gene Therapy (SR-Tiget), via Olgettina 60, 20132 Milan, Italy. E-mail: villa.anna@hsr.it. Or: Luigi D. Notarangelo, MD, National Institute of Allergy and Infectious Diseases, National Institutes of Health, 10 Center Drive, Bethesda, MD 20892. E-mail: luigi.notarangelo2@nih.gov.

0091-6749

https://doi.org/10.1016/j.jaci.2020.04.005

Conclusions: These results support the existence of an interplay between gut and skin that can sustain skin inflammation in OS. (J Allergy Clin Immunol 2020;■■■:■■■-■■■.)

Key words: *RAG, T cells, skin inflammation, erythroderma, immune-mediated disease, cytokines, chemokines, gut-skin axis, LPS, dysbiosis*

Maintenance of skin homeostasis relies on the crosstalk among epidermal keratinocytes, resident immune cells, and commensal microbiota. Breaching of the cutaneous barrier and inadequate or excessive immune response to microbial challenges potentially lead to chronic inflammation and autoimmunity.[1] A large number of T cells normally populate the skin, providing immune surveillance. In addition to this resident population, a subset of recirculating memory T cells has been identified, contributing to widespread immune protection of distal lymphoid and cutaneous tissues.[2,3] Migration of T cells into the skin requires ligands for E- and P-selectin, among which an important role is played by the P-selectin ligand CD162, also known as cutaneous lymphocyte antigen (CLA).[4] Moreover, skin-homing T cells express the chemokine receptors CCR4 and CCR10, whose ligands —chemokine C-C motif ligands (CCL)17, CCL22, and CCL27 —are upregulated in the dermal vasculature and in epidermal keratinocytes in many inflammatory conditions.[5-7] Imprinting of skin-homing properties in T cells critically depends on skin-derived dendritic cells (DCs); T cells activated in skin-draining peripheral lymph nodes (PLNs) express higher levels of selectin ligands than those activated in mesenteric lymph nodes (MLNs).[5] Conversely, the gut-homing receptors α4β7 and CCR9 are preferentially induced when T cells are activated in MLN.[8] Thus, in general, effector T cells trafficking to the skin are devoid of gut-homing molecules and gut-tropic cells do not express skin-homing molecules. Nonetheless, evidence of plasticity in the homing phenotype has been accumulating in the context of inflammation.[9]

Cutaneous manifestations are common in patients with primary immunodeficiency disease.[10,11] Omenn syndrome (OS) is a severe immunodeficiency most often caused by hypomorphic mutations in the *RAG* family, leading to generation of oligoclonal T cells that expand in the periphery and infiltrate various organs, particularly barrier tissues such as skin and gut.[12] The most distinctive clinical feature of OS is a generalized exfoliative erythroderma with onset at neonatal age, associated with alopecia, lymphadenopathy, hepatosplenomegaly, recurrent and severe infections, and failure to thrive.[12] Skin biopsies from patients with OS reveal massive T-cell infiltration and an aberrant distribution of Langerhans cells, indicating that immune abnormalities play an important role in the skin disease pathophysiology.[13,14] Patients with OS also frequently suffer from chronic diarrhea, and biopsies of the gastrointestinal tract reveal prominent T-cell and eosinophil infiltrates in the lamina propria, villous flattening in the small bowel, and cryptitis in the colon.[15] A close association between skin disease and microbiota (not limited to skin microbiota) has been demonstrated. For instance, atopic dermatitis (AD) and rosacea are both linked to changes in the gut barrier and intestinal microbiota.[16] Reduced microbial diversity was reported in infants with eczema.[17,18] Furthermore, a link between imbalances of the intestinal microbial communities and development of skin psoriasis has been documented in mice and patients.[19] We have recently demonstrated that intestinal microbiota play a major role in the immune dysregulation of the 129Sv/C57BL/6 knock-in *Rag2*$^{R229Q/R229Q}$ (*Rag2*^{R229Q}) mouse model of OS, leading to the systemic dissemination of gut-derived proinflammatory T_H1/T_H17 cells.[20] Whether such alterations in gut homeostasis may also influence the cutaneous manifestations of OS is not known.

Here, we provide evidence supporting a role for gut-skin axis in the pathophysiology of OS. We found that compromised skin barrier integrity in *Rag2*^{R229Q} mice results in altered microbial load and composition and dysregulated production of T cell–recruiting chemokines by activated epithelial cells. Importantly, intestinal inflammation and gut barrier leakage synergistically support the activation of skin epithelial cells and the recruitment of T cells to the skin. An increased proportion of circulating T cells expressing skin-homing receptors and elevated plasma levels of LPS and skin chemoattractants have been also documented in patients with OS, suggesting that mechanisms similar to those observed in the mouse model may also operate to induce skin inflammation in humans.

Abbreviations used

Actb:	Housekeeping gene β-actin
AD:	Atopic dermatitis
CCL:	Chemokine C-C motif ligand
CLA:	Cutaneous lymphocyte antigen
CXCL:	C-X-C motif chemokine ligand
DC:	Dendritic cell
DLN:	Draining lymph node
DSS:	Dextran sulfate sodium salt
EB:	Evans blue dye
FACS:	Fluorescence-activated cell sorting
HD:	Healthy donor
H&E:	Hematoxylin and eosin
MLN:	Mesenteric lymph node
OS:	Omenn syndrome
OT:	OVA transgenic mouse
OVA:	Ovalbumin
PLN:	Peripheral lymph nodes
Rag2^{R229Q}:	129Sv/C57BL/6 knock-in *Rag2*$^{R229Q/R229Q}$
TLR:	Toll-like receptor
WT:	Wild type

METHODS

Human studies

Patient's samples were collected with the informed consent of their parents, according to protocol 18-I-0041 approved by the National Institutes of Health institutional review board and protocols TIGET06 and TIGET09 approved by the San Raffaele Scientific Institute ethics committee. Table E1 (in the Online Repository available at www.jacionline.org) describes clinical, immunological, and molecular features of 15 unrelated patients with OS. A cohort of age-matched healthy donors (HDs), patients with acute graft-versus-host disease and patients with AD were also studied as controls. PBMCs from peripheral blood were purified on Ficoll gradient (Lympholyte cell separation media; Cedarlane Laboratories, Burlington, Ontario, Canada).

Mice

The *Rag2*^{R229Q} mice were previously described.[20] The colony was maintained in a specific pathogen–free facility in heterozygosity and littermates

were kept in the same cage until weaning. Both male and female mice between 8 and 12 weeks old were used for experiments. OVA transgenic OT-I and OT-II mice were obtained from Charles River Laboratories (Wilmington, Mass). The animal procedures were approved by the Istituto Clinico Humanitas, according to the Italian Institutional Animal Care and Use Committee and European Union directive for animal experiments. Details about the experimental design, *in vivo* procedure, and treatments are described in the supplementary Methods in this article's Online Repository at www.jacionline.org.

ELISA tests

Quantification of mouse Ccl17 and Ccl22 and human CCL17, CCL22, and C-X-C motif chemokine ligand (CXCL)-10 were determined with ELISA kits (R&D Systems, Minneapolis, Minn), according to manufacturer's instructions. Human LPS-binding protein was determined in the sera of patients with OS and age-matched HDs using human LBP ELISA kit (MyBioSource, San Diego, Calif), used according to manufacturing's instructions.

Quantification of adherent bacteria to cutaneous epithelium

One centimeter of skin biopsies was collected from age- and sex-matched mice using sterile conditions and digested in lysis buffer (10 mmol/L TRIS, 100 mmol/L NaCl, 10 mmol/L EDTA, 0.5% SDS, and 0.4 mg/mL proteinase K). Total DNA was extracted with the isopropanol-ethanol method. The microbial load was determined with real-time quantitative PCR (SYBR green) using 16S and 18S ribosomal RNA gene-specific probes.[20]

Mouse cutaneous cell preparation

Skin tissue was digested with Liberase TL (0.45 mg/mL; Roche, Basel, Switzerland) for 1 hour at 37°C. Cell suspension was washed, passed through a 100-μm cell strainer, and analyzed by flow cytometry,

Lymph flow assessment using EB

Three μL of 1% Evans blue dye (EB) solution in PBS was injected into the back of anesthetized mice using a Hamilton syringe (Hamilton Company, Reno, Nev). After 16 hours mice were sacrificed. EB was extracted from the skin biopsies of the back by incubating them at 55°C for 5.5 hours in formamide (Honeywell Fluka, Thermo Fisher Scientific, Waltham, Mass). The absorbance was measured with microplate reader at 620 nm. The dye concentration was calculated from a standard curve of EB in formamide (Sigma-Aldrich, St Louis, Mo) and is represented as absolute amount of dye remaining in the skin tissue.

Flow cytometry

Cell suspensions obtained from mouse organs were preincubated with FcγR-specific blocking antibodies (eBioscience, San Diego, Calif) and stained with the following antibodies from eBioscience: TCR-γδ (UC7-13D5), CD45 (30-F11), CD4 (RM4-5), CD8a (53-6.7), CCR9 (CW-1.2), CD103 (2E7), CD11C (N418), MHCII (M5/114.15.2), CCR4 (2G12), IL-17A (17B7) and IFN-γ (XMG1.2). Dead cells exclusion was performed with Aqua Cell Stain kit (Invitrogen, Thermo Fisher Scientific). For intracellular staining, cells were stimulated for 4 hours with phorbol 12-myristate 13-acetate (5 ng/ml; Sigma-Aldrich) and ionomycin (1 μg/ml; Sigma-Aldrich). Golgi stop (1000×; BD, Franklin Lakes, NJ) was added during the last 3 hours of stimulation. Cell fixation and permeabilization was performed using the Fixation and Permeabilization Buffer kit (eBioscience). Human cells were stained with the following antibodies from BioLegend (San Diego, Calif): CD4 (OKT4), CD8 (RPA-T8), CD45RA (HI100), CD45RO (UCHL1), CLA (HECA-452), CCR4 (L291H4). Fluorescence-activated cell sorting (FACS) data were acquired with FACSCanto II (BD) and analyzed with FlowJo software (version 9.9.6; Tree Star, BD).

Real-time PCR

Cutaneous tissues (1 cm^2) were homogenized in PureZOL reagent (Bio-Rad Laboratories, Hercules, Calif) using TissueLyzer II (QIAGEN, Hilden, Germany). RNA was extracted using RNeasy Lipid Tissue kit (QIAGEN). A total of 1 μg of RNA was used to synthetize cDNA using the High-Capacity cDNA Reverse Transcription kit (Applied Biosystems, Foster City, Calif). Gene expression was investigated by SYBR green RT-qPCR using the CFX384 system (Bio-Rad). The housekeeping gene β-actin (Actb) ribosomal RNA was used as control. List of primers are available in Table E2 in this article's Online Repository at www.jacionline.org.

Histology and immunohistochemistry

Mouse tissue samples were formalin-fixed and paraffin-embedded. Sections (1.5 μm) were used for routine hematoxylin and eosin (H&E) analysis and staining with primary antibodies. Arbitrary gut and skin histological score was calculated in a double-blind study by a pathologist. Scoring from 0 to 3 (where 0 is normal condition and 3 is severe structural changes) was adopted for evaluating different manifestations in each tissue. Detailed description of histological and morphometric analyses are described in the supplementary Methods in the Online Repository.

In situ RNA hybridization

In situ hybridization for IFN-γ, CXCL9, and CXCL10 on formalin-fixed paraffin-embedded samples was performed using the RNAscope 2.5 HD Assay-BROWN (Advanced Cell Diagnostics, Newark, Calif) according to the manufacturer's instructions. POLR2A mRNA labelling was used as positive control for the RNA quality in samples. Staining procedure is described in the supplementary Methods in the Online Repository.

Statistical analysis

Statistical analysis was conducted using GraphPad Prism software (GraphPad Software Inc, La Jolla, Calif). Results were analyzed using the nonparametric Mann-Whitney test or the ANOVA with multiple comparisons test. Data are generally shown as mean ± SEM unless otherwise stated. Value of $P < .05$ was considered significant.

RESULTS

Enhanced skin tropism of PB memory T cells in patients with OS

Erythroderma, with skin infiltration by autoreactive and oligoclonal autologous T cells, represents the clinical hallmark of OS. CLA controls the influx of memory T cells to cutaneous sites.[21] We studied 15 patients with OS due to *RAG* mutations (Table E1) and 37 healthy infants (HDs) and examined CLA expression in PB T cells. In both CD4 and CD8 effector/memory $CD45R0^+$ T cell subsets, the frequency of CLA^+ cells was dramatically increased in patients with OS compared with age-matched HDs (Fig 1, *A*). Circulating CLA^+ T cells coexpress the chemokine receptor CCR4 and rely on T-cell chemoattractant CCL22 and CCL17 to reach the inflamed skin.[5,22] Indeed, CCR4 was expressed on almost the totality of $CD4^+$ $CD45RA^-$ cells in patients with OS (Fig 1, *A*), and higher levels of the CCR4 ligands CCL17 and CCL22 were detected in the plasma, as compared to HDs (Fig 1, *B*). These features are consistent with the T_H2 phenotype of OS, as also indicated by elevated serum levels of IL-5 and IL-13 (Fig 1, *C*). Surprisingly, we found that patients with OS

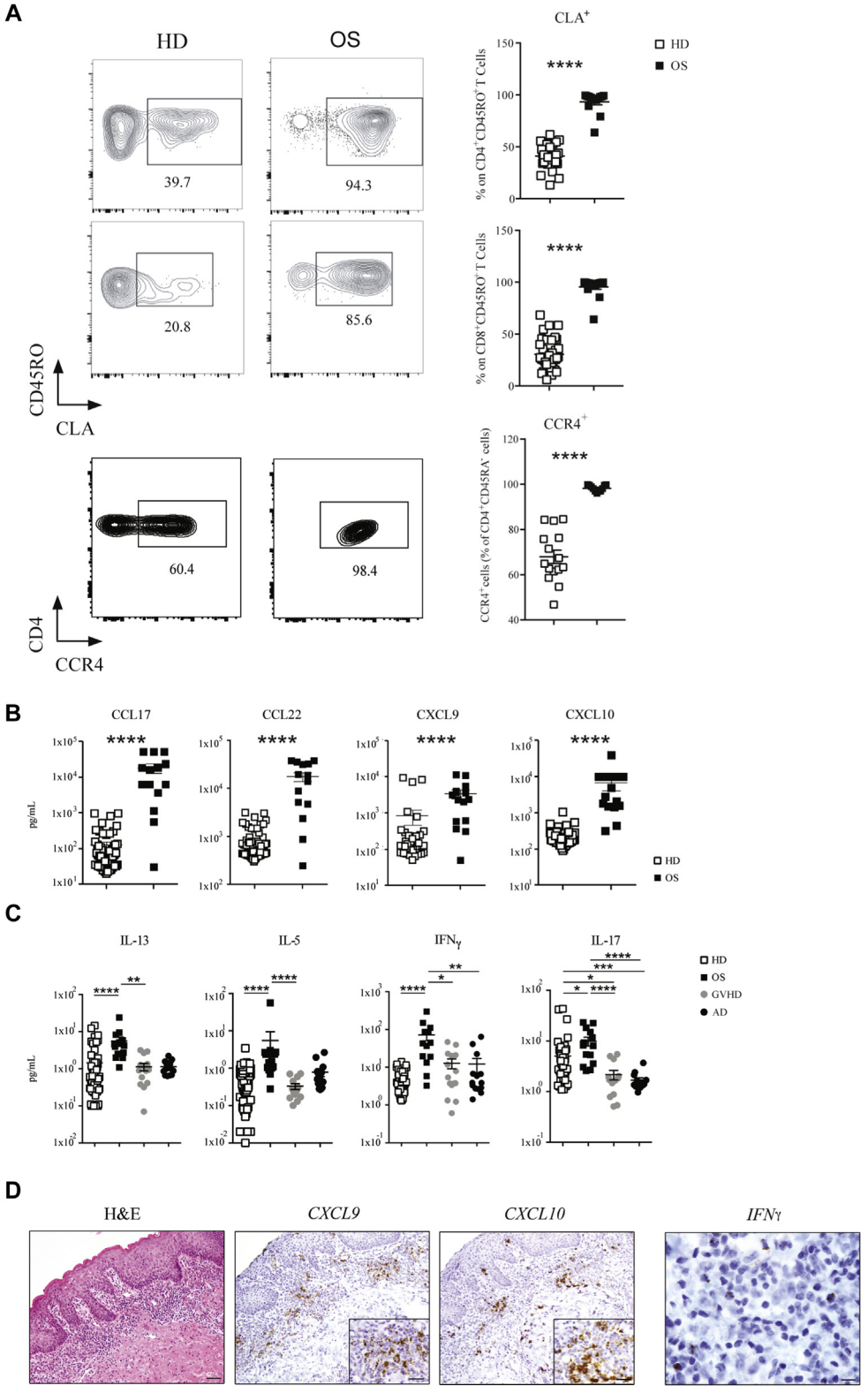

FIG 1. Preferential homing of T cells to the skin in patients with OS. **A,** Representative FACS plots and frequencies of CLA^+ $CD45RO^+$ T cells within the effector $CD4^+$ and $CD8^+$ T-cell populations isolated from PB of patients with OS (n = 13) and aged-matched HDs (n = 31). Frequencies of $CCR4^+$ within the $CD4^+$ $CD45RA^-$ T-cell population (n = 11-15). Plasma levels of chemokines (**B**) and cytokines (**C**) in HDs (n = 37), in patients with OS (n = 15) as well as in patients with acute graft-versus-host disease (*GvHD*) (n = 15) and patients with AD (n = 14), as controls of T_H1- and T_H2-mediated inflammation, respectively. **D**, Skin biopsies from patients with OS were investigated for *IFNG*, *CXCL9,* and *CXCL10* mRNA expression using RNAscope. POLR2A mRNA labeling was used as control for the quality of the RNA on paraffin section. Values are mean ± SEM. $*P < .05$, $**P < .01$, $***P < .005$, $****P < .001$. Statistical significance determined by Mann-Whitney *U* test or by ANOVA. See also Table E1.

exhibited also significantly high plasma levels of IFN-γ and IFN-γ–inducible chemokines CXCL9 and CXCL10, as well as of IL-13, IL-5, and IL-17 (Fig 1, *B* and *C*). Furthermore, plasma levels of T_H1 and T_H2 cytokines were significantly higher in patients with OS than in patients with graft-versus-host disease and AD, 2 prototypic conditions characterized by T_H1 and T_H2 skewing, respectively (Fig 1, *C*). Altogether, these data indicate that the inflammation of OS is characterized by a systemic and broad signature. Consistent with this, *IFNG* and to greater extent *CXCL9* and *CXCL10* mRNA signals were readily detected in skin biopsies from patients with OS (Fig 1, *D* and Fig E1 in this article's Online Repository at www.jacionline.org).

Skin inflammation in *Rag2*^{R229Q} mice is characterized by T-cell infiltration and a T_H1-biased cytokine response

To investigate specifically the pathophysiology of skin disease in OS, we used the *Rag2*^{R229Q} mouse model.[14,23] Typically, mutant mice develop epidermal hyperplasia, hyperkeratosis, and dermal immune cell infiltration (Fig 2, *A* and *B*). Such alterations, associated with massive signs of subcutaneous hemorrhage and PLN enlargement, were much more pronounced in mice with overt skin erythroderma (Fig E2 in this article's Online Repository at www.jacionline.org). Immunophenotypic analysis of the skin infiltrate confirmed an expansion of mononuclear $CD45^+$ cells, particularly of $CD4^+$ and $CD8^+$ T cells (Fig 2, *C* and *D*). Moreover, the cutaneous expression of the chemokine receptor *Cxcr3* was increased in mutant mice (Fig 2, *E*). Consistent with this, $CD3^+$ T cells isolated from the skin of *Rag2*^{R229Q} mice displayed much higher frequencies of Ifn-γ–producing cells on phorbol 12-myristate 13-acetate and ionomycin pulsing than those from wild-type (WT) control mice (Fig 2, *F*). Of note, the proportion of Il-17–producing cells in mutant mice was comparable to what observed in controls, despite lack of Tcrγδ$^+$T cells, the main producers of this cytokine in the skin (Fig 2, *F* and *G*).

Rag2^{R229Q} mice exhibit dysfunction of the epidermal barrier and increased microbial challenge

At steady state, the epidermis of *Rag2*^{R229Q} mice appears thickened compared with the epidermis of WT mice (Fig 3, *A*). Expression of the epidermal differentiation markers, cytokeratin 5 (*Ck5*) and loricrin, was markedly increased (Fig 3, *B*). Similarly, the mRNA level of the hyperproliferative/wound-associated cytokeratin 6 (*Ck6*) was also augmented (Fig 3, *B*), overall indicating an altered keratinocyte differentiation program. Antimicrobial peptides are significantly upregulated in mouse models with altered skin barrier.[24,25] We found that cutaneous expression of cathelin-related antimicrobial peptides (*Cramp*) and β-defensin 3 (*mβ-d3*) was increased in *Rag2*^{R229Q} mice (Fig 3, *C*). Furthermore, mutant mice exhibited augmented tissue expressions of several Toll-like receptors (*Tlrs*) as well as of the downstream adaptor molecules, myeloid differentiation primary response 88 (*MyD88*) and TIR-domain–containing adapter-inducing IFN-β (*Trif*) (Fig 3, *D* and *E*), suggestive of disturbance in the cutaneous barrier integrity and increased microbial challenge. In line with this, skin bacterial load was increased in *Rag2*^{R229Q} mice (Fig E3, *A* in this article's Online Repository at www.jacionline.org), indicating a possible expansion of the overall number of bacteria compared with in their WT littermates. Notably, 16S ribosomal RNA gene sequencing revealed that bacterial taxonomic richness was generally reduced in the skin of *Rag*-mutant mice (Fig E3, *B*), with lower abundance of *Propionibacterium* (P_{adj} < .028), *Bacteroides* (P_{adj} < .009), and *Staphylococcus* (P_{adj} < .008) (Fig E3, *C*) genera, which are cutaneous commensal bacteria contributing to maintenance of tissue homeostasis.[26]

Following the observation that cutaneous Toll-like receptor 4 (Tlr4) expression was markedly upregulated in *Rag2*^{R229Q} mice, we examined further the effect of local Tlr4 activation. Mice received a single intradermal injection of 100-μg LPS on the right portion of the back and of PBS on the left and were sacrificed 24 hours later. Hemorrhage and dermal tissue necrosis were evident at the LPS injection site in almost all treated mutant mice (Fig 3, *F*). In particular, histopathology of skin sections revealed widespread epidermal thickening with hyperkeratosis and increased abscess formation and hemorrhage. By contrast, WT mice showed mild signs of hemorrhage and no microabscesses (Fig 3, *F*). We also analyzed the expression of the CK6-inducing cytokine *Il-1β*[27] as well as of *Ifng*, involved in the pathogenesis of inflammatory skin diseases.[28] Expression of both cytokines was strongly induced in the skin of *Rag2*^{R229Q} mice in response to LPS (Fig 3, *G*). Moreover, the augmented expression of the keratinocyte-derived *Cxcl2* chemokine correlated with a robust recruitment of innate cells to the skin of *Rag2*^{R229Q} mice (Fig 3, *G*). Thus, *Rag2*^{R229Q} mice are more susceptible to LPS-induced cutaneous inflammation.

Chronic skin inflammation sustains immune cell infiltration in *Rag2*^{R229Q} mice

Chronic microbial stimulation may induce keratinocyte activation.[29-31] Skin epithelial cells of *Rag2*^{R229Q} mice expressed high levels of MHC class II molecules (Fig 4, *A*). Moreover, the expression of several cytokines, including Ifn-γ, Tnf-α, Il-23, Il-1β, Il-5, Il-13, Il-33, and thymic stromal lymphopoietin (Tslp), was significantly upregulated in the mutant skin (Fig 4, *B*), suggesting that these cytokines may contribute to skin inflammation, without an obvious skewing of T_H responses. Consistent with this, levels of both T_H1 (Cxcl9, Cxcl10) and T_H2 (Ccl20, Ccl22, and Ccl17)-related chemokine transcripts were markedly increased in the skin of *Rag2*^{R229Q} mice (Fig 4, *C*). Levels of Ccl17 and Ccl22 were also elevated in the serum of *Rag*^{R229Q} mice (Fig 4, *D*), correlating with a higher frequency of Ccr4-expressing skin homing $CD3^+$ T cells detected in the PLNs, spleen, and MLNs (Fig 4, *E*). Overall, these data mirror what is observed in patients with OS (Fig 1) and suggest a broad inflammatory signature in this disease.

To test whether this inflammatory environment has a role in promoting antigen-driven cutaneous T-cell migration, we adoptively transferred $CD4^+$ or $CD8^+$ lymphocytes from OT-II or OT-I mice into *Rag2*^{R229Q} and *Rag2*$^{+/+}$ recipients. Then, we topically immunized the ear pinna once with ovalbumin (OVA) plus cholera toxin, and after 7 days, treated mice were sacrificed. Epicutaneous challenge caused marked epidermal changes in *Rag2*^{R229Q} mice, with enhanced vascularization and dermal infiltration by immune cells (Fig E4, *A-C* in this article's Online Repository at www.jacionline.org). Accumulation of transgenic T cells was significantly increased within the cervical LNs (Fig E4, *D* and *E*) and skin (Fig E4, *F* and *G*) of immunized *Rag2*^{R229Q} mice compared with that of controls. Overall, these findings

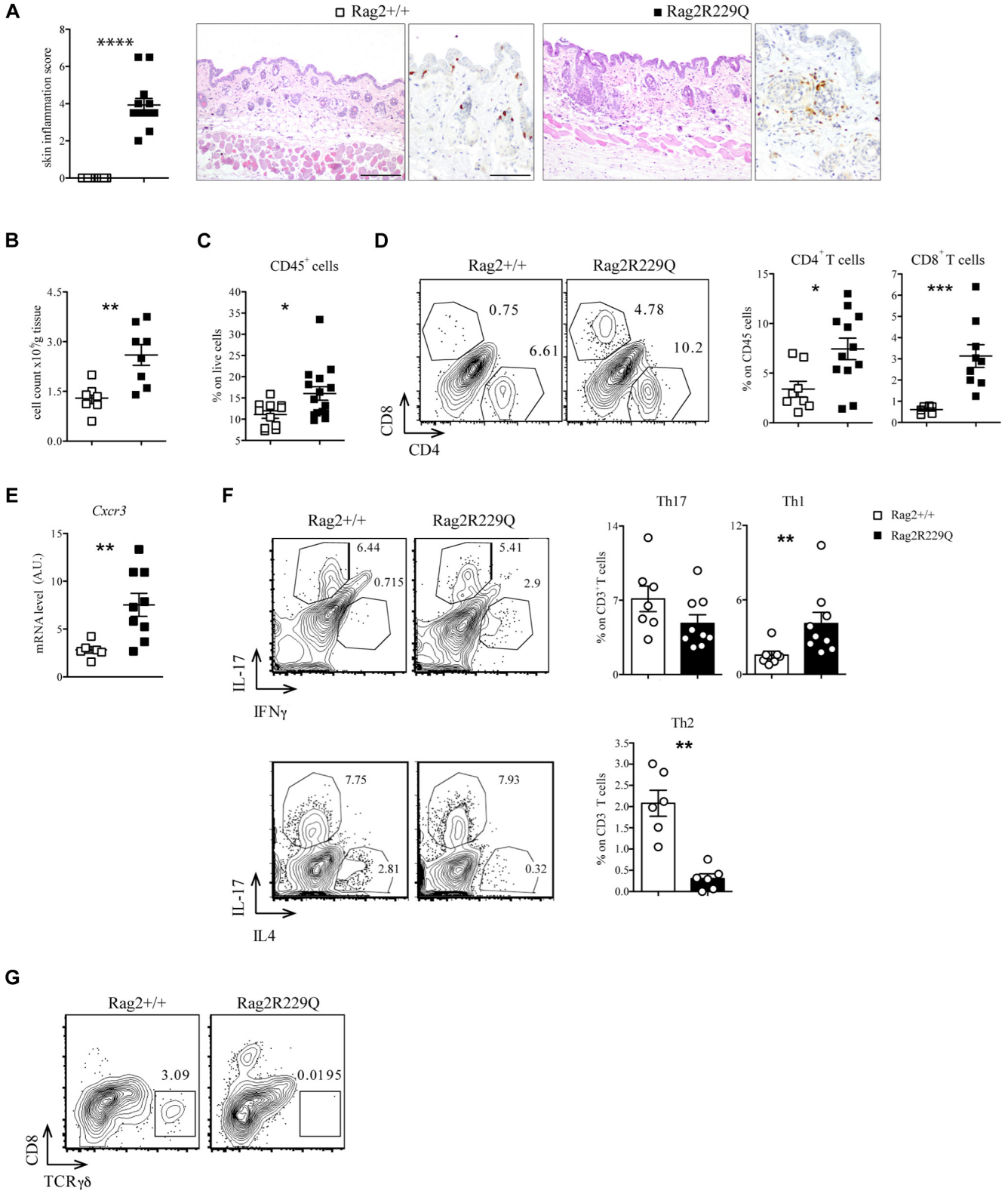

FIG 2. *Rag2*^{R229Q} mice exhibit severe T-cell–mediated inflammation in the skin. **A,** Representative skin sections from *Rag2*$^{+/+}$ and *Rag2*^{R229Q} mice (8-12 weeks old) stained with H&E and CD3 immunostaining. Histogram shows the inflammation score in the skin (n = 12-13). Bars = 200 μm (H&E) and 100 μm (CD3). **B,** Total cell count from skin suspension for g tissue (n = 7-8 mice/group). **C,** Frequencies of CD45$^+$ cells in the skin suspension (n = 9-10 mice/group). **D,** Representative FACS plots and cumulative frequencies of CD4$^+$ and CD8$^+$ T cells inside the CD45$^+$ population of skin suspension (n = 6-12 mice/group). **E,** Gene expression analysis of *Cxcr3* in the skin tissue of *Rag2*$^{+/+}$ and *Rag2*^{R229Q} mice (n = 6-9 mice/group). Target mRNA was normalized to *Actb* mRNA. RNA contents are shown as arbitrary units (*AUs*). **F,** Representative FACS plots and frequencies of T_H1, T_H17, and T_H2 cells inside the CD3$^+$ T-cell population of skin suspension (n = 6-9 mice/group). **G,** Representative FACS plots showing TCRγδ T cells inside the CD45$^+$ population in the skin of *Rag2*$^{+/+}$ and *Rag2*^{R229Q} mice. Values are mean ± SEM. **P* < .05; ***P* < .01; ****P* < .005; *****P* < .001. Statistical analysis was performed using Mann-Whitney *U* test. See also Fig E1.

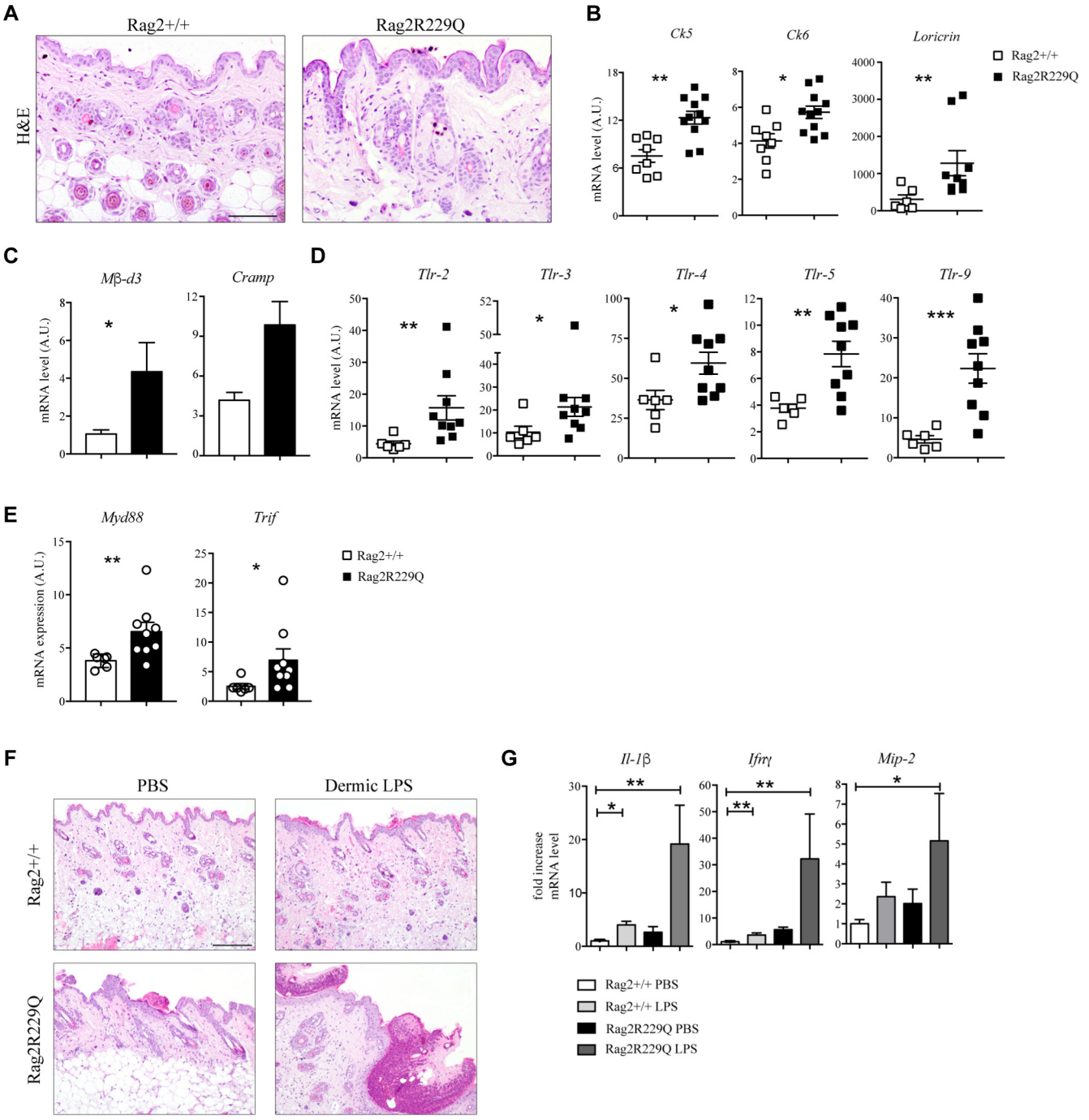

FIG 3. Altered barrier integrity and microbial load characterized the skin of *Rag2*^{R229Q} mice. **A,** Representative skin sections from *Rag2*$^{+/+}$ and *Rag2*^{R229Q} mice stained with H&E. Bar = 100 μm. **B,** Cutaneous gene expression analysis of keratins (*Ck5-Ck6*) and Loricrin in *Rag2*$^{+/+}$ and *Rag2*^{R229Q} mice (n = 8-11 mice/group from 3 experiments). Target mRNA was normalized to Actb mRNA. RNA contents are shown as AUs. **C,** Gene expression analysis of *Mβ-d3* and *Cramp* in the skin tissue (n = 4-8 mice/group). Gene expression analysis of *Tlrs* (**D**) and *Myd88* and *Trif* (**E**) in the skin tissue of *Rag2*$^{+/+}$ and *Rag2*^{R229Q} mice (n = 6-9 mice/group). Target mRNA was normalized to *Actb* mRNA. RNA contents are shown as AUs. **F,** *Rag2*$^{+/+}$ and *Rag2*^{R229Q} mice received a single intradermal injection of 100 μg LPS on the left and PBS on the right portion of the back. Mice were then sacrificed 24 hours later. Representative skin sections from dermal LPS-treated and untreated *Rag2*$^{+/+}$ and *Rag2*^{R229Q} mice stained with H&E. Bar = 200 μm. **G,** Fold increase of *Il-1β*, *Ifng,* and macrophage inflammatory protein 2 (*Mip-2*, also known as*Cxcl2*) on skin tissue. Data are representative results of 3 independent experiments with at least 6 mice/group. Values are mean ± SEM. **P* < .05; ***P* < .01; ****P* < .005. Statistical analysis was performed using Mann-Whitney *U* test.

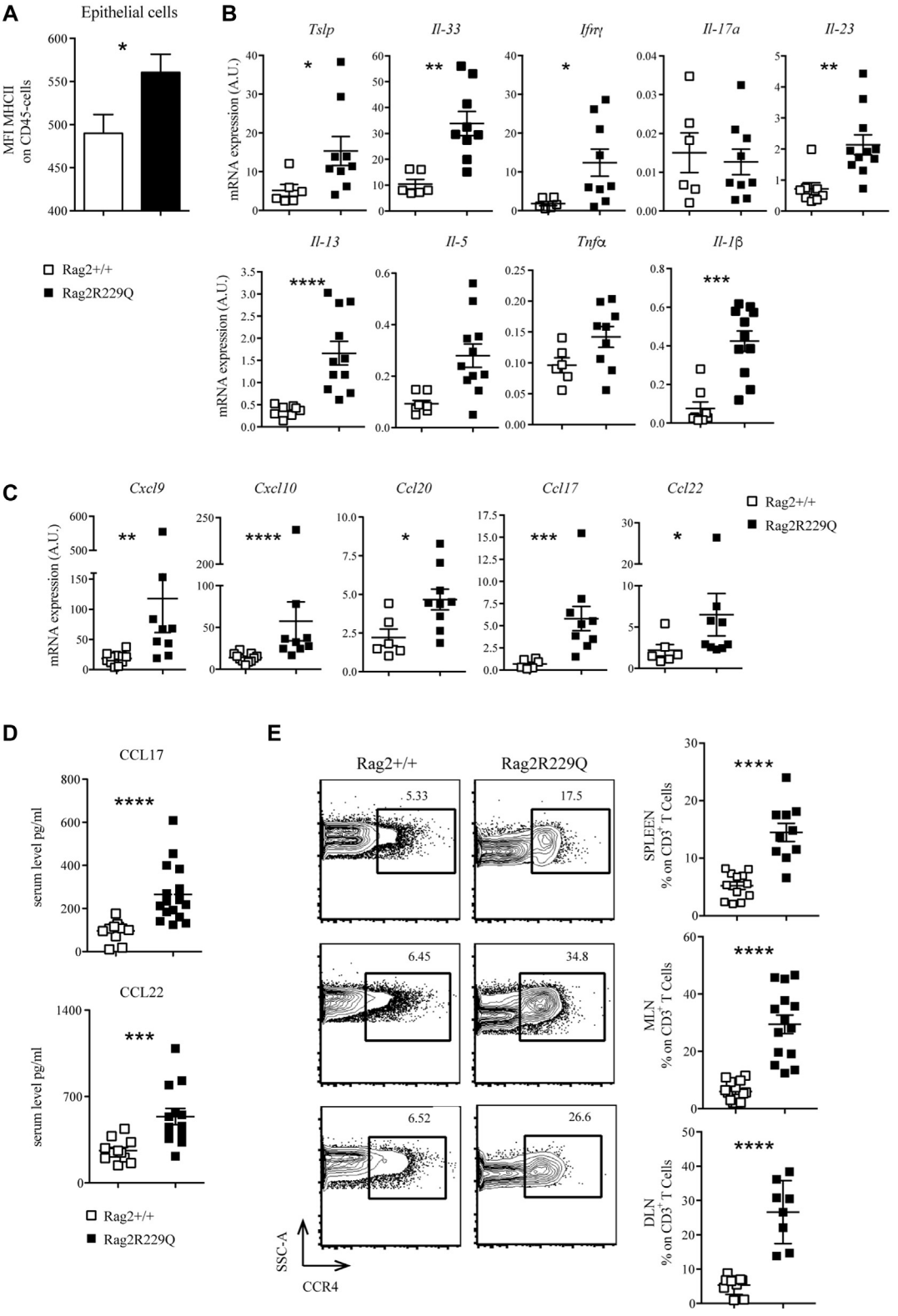

FIG 4. Characterization of cutaneous inflammatory environment in *Rag2*^{R229Q} mice. **A,** Mean fluorescence intensity (MFI) for MHCII expression among CD45$^-$ population of skin suspension (n = 6-7 mice/group). Transcriptional analysis of several cytokines (**B**) and chemokines (**C**) in the skin tissue (n = 6-9 mice/group from 3 experiments). Target mRNA was normalized to *Actb* mRNA. RNA contents are shown as AUs. **D,** Levels of the chemokines Ccl17 and Ccl22 in the serum of *Rag2*$^{+/+}$ and *Rag2*^{R229Q} mice (n = 12-13 mice/group from 3 experiments). **E,** Representative FACS plots and cumulative frequencies of CCR4$^+$ inside the CD3$^+$ T-cell population of spleen, MLN, and DLN (n = 14 mice/group from 3 experiments). Values are mean ± SEM. **P* < .05; ***P* < .01; ****P* < .005; *****P* < .001. Statistical analysis was performed using Mann-Whitney *U* test. See also Fig E3. *SSC-A*, Side scatter.

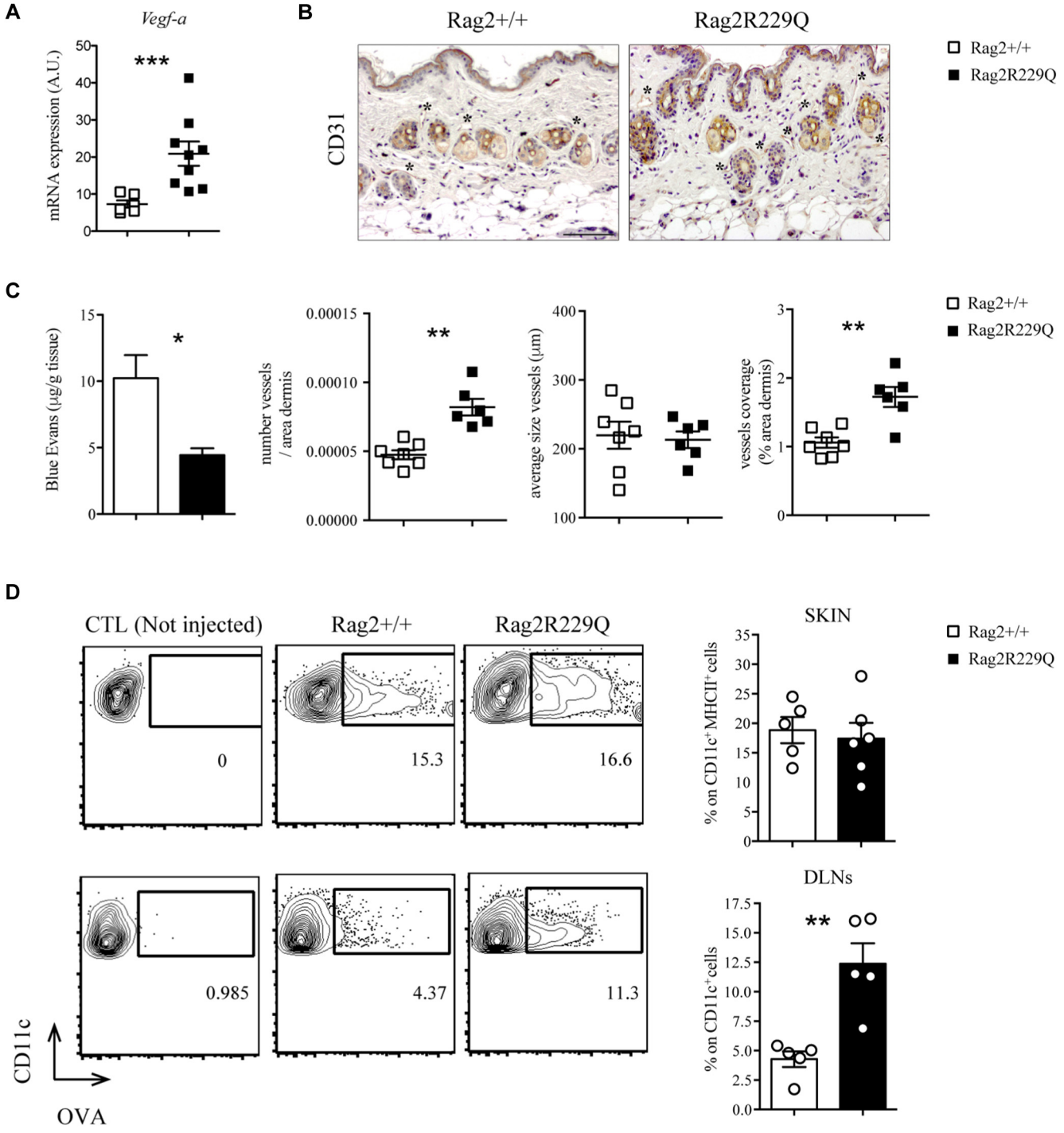

FIG 5. Increased DC trafficking from the skin of *Rag2*^{R229Q} mice. **A,** Gene expression analysis of *Vegfa* in the skin tissue of *Rag2*$^{+/+}$ and *Rag2*^{R229Q} mice (n = 6-9 mice/group from 3 experiments). **B,** Representative skin sections stained with CD31. Bar = 100 μm. The evaluation of several parameters was performed by computer-assisted morphometric analysis of CD31-stained skin sections (n = 5 mice/group). **C,** Quantification of extracted EB from the back skin of *Rag2*$^{+/+}$ and *Rag2*^{R229Q} mice, normalized to tissue weight (g). Data are representative results of 3 independent experiments with at least 4 mice per group. **D,** Allophycocyanin-labeled OVA antigen was intradermally injected in the ears of *Rag2*$^{+/+}$ and *Rag2*^{R229Q} mice, and its uptake by DCs was evaluated in the skin and DLNs after 6 hours. Representative dot plots and frequencies of OVA-loaded DCs from skin (CD11c^{+} MHCII^{+}) and DLNs (CD11c^{+}) of OVA-injected *Rag2*$^{+/+}$ and *Rag2*^{R229Q} and negative control (not injected). Data are representative results of 3 independent experiments with at least 5 mice per group. Values are mean ± SEM. **P* < .05; ***P* < .01; ****P* < .005. Statistical analysis was performed using unpaired Student's *t* test and Mann-Whitney *U* test. *CTL*, Control.

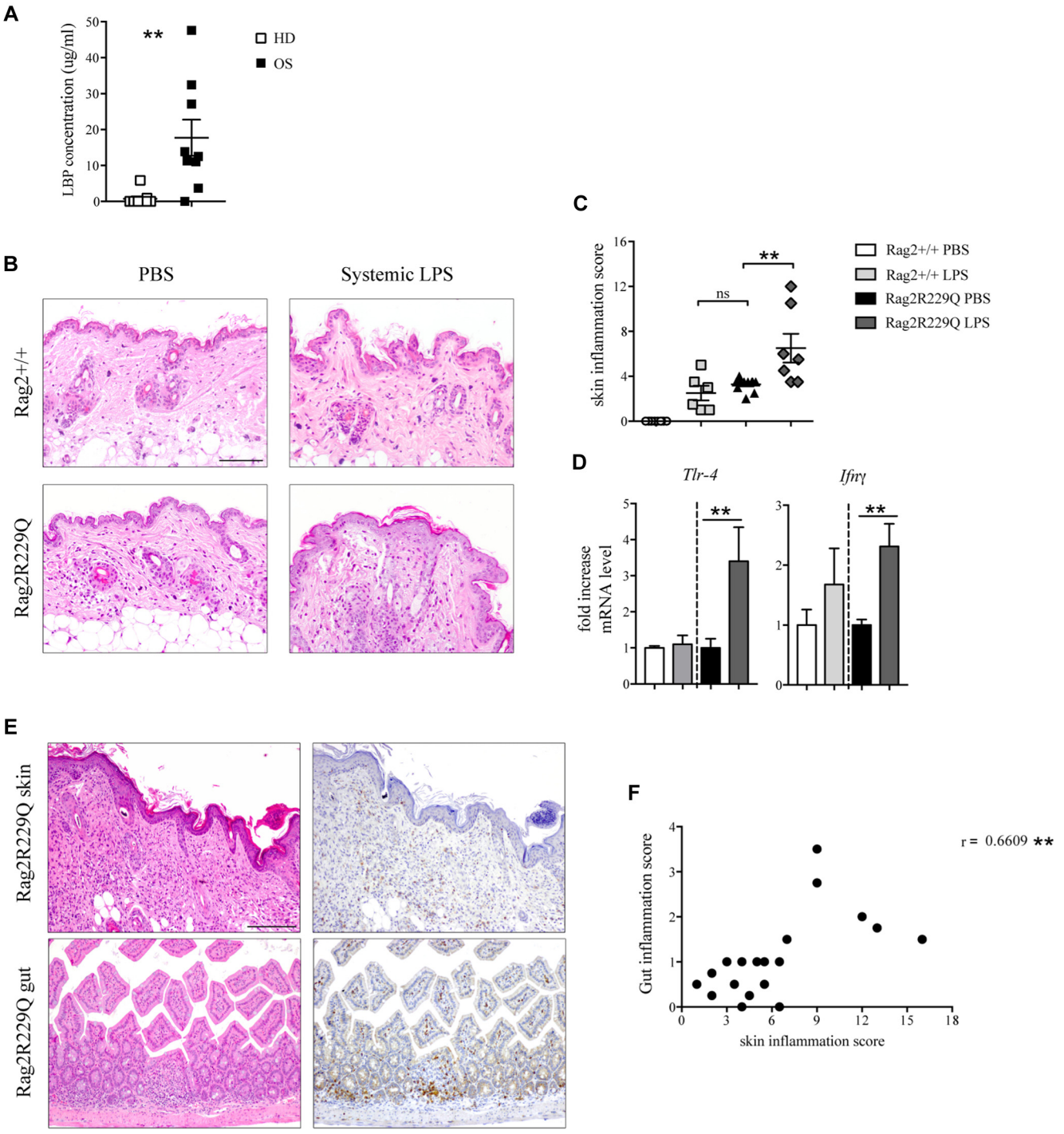

FIG 6. Systemic LPS triggers cutaneous inflammation. **A,** LPS-binding protein (*LBP*) concentration in the sera of patients with OS and HDs (n = 8-9 from 2 experiments). **B,** *Rag2*$^{+/+}$ and *Rag2*^{R229Q} mice received a single injection of 100 μg LPS intraperitoneally and were sacrificed 24 hours later. Representative skin sections from systemic LPS-treated and untreated *Rag2*$^{+/+}$ and *Rag2*^{R229Q} mice stained with H&E. Bar = 200 μm. **C,** Histogram shows the inflammation score in the skin of n = 6-11 mice/group from 2 experiments. **D,** Fold increase of *Ifng* and *Tlr4* on skin tissue (n = 6-8 mice/group from 2 experiments). **E,** Representative small intestinal and skin sections from *Rag2*^{R229Q} mice with erythroderma stained with H&E and CD3 immunostaining. Bar = 200 μm. **F,** Correlation between intestinal and skin inflammation scores of *Rag2*^{R229Q} mice manifesting or not evident cutaneous manifestations (*black dots*). The Spearman *r* value is indicated in the graph (n = 10 mice). Values are mean ± SEM. $^{**}P < .01$. Statistical analysis was performed using Mann-Whitney *U* test.

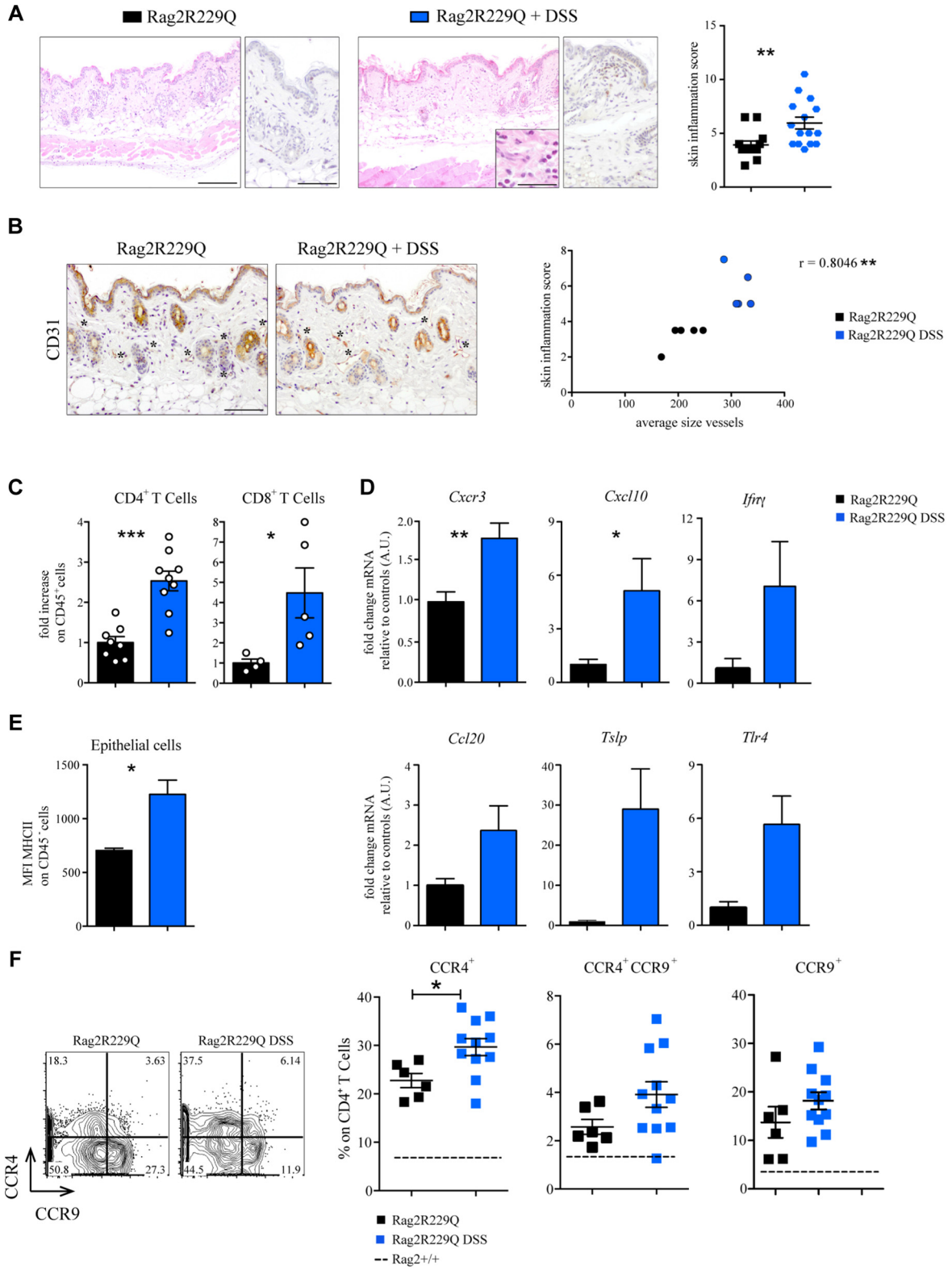

FIG 7. Boosted intestinal inflammation worsens skin inflammation in *Rag2*^{R229Q} mice. **A,** Colitis in *Rag2*^{R229Q} mice was induced by cyclic DSS administration. Representative skin sections stained with H&E and CD3 immunostaining. Bars = 200 μm (H&E) and 100 μm (CD3). Higher magnification shows eosinophils. Bar = 50 μm. Histogram shows the inflammation score in the skin (n = 12-15 mice/group from 3 experiments). **B,** Representative skin sections from untreated and DSS-treated *Rag2*^{R229Q}mice stained with CD31 immunostaining (*asterisks* mark the CD31-positive vessels). Bar = 100 μm. Correlation between cutaneous inflammation and average vessels size of untreated *Rag2*^{R229Q} (*black dots*) and DSS-treated

indicate that keratinocyte activation and cutaneous inflammatory environment in mutant mice contribute to T-cell skin homing and infiltration.

Enhanced peripheral trafficking of skin-derived DCs in *Rag2*^{R229Q} mice

Cell trafficking to inflamed tissues is influenced by vascular remodeling.[32] We found that levels of the angiogenic vascular endothelial growth factor A (Vegfa) were elevated, and CD31$^+$ endothelial cells were present at higher number and density in the skin of *Rag2*^{R229Q} mice (Fig 5, *A* and *B*). To investigate possible abnormalities of lymphatic vessels, we quantified the uptake and drainage of the lymphatic tracking dye EB after intradermal injection into the back skin.[33] Significantly less EB remained localized within the skin of *Rag2*^{R229Q} compared with in WT mice, indicating enhanced lymphatic clearance (Fig 5, *C*). Hence, trafficking of antigens and immune cells from the skin of *Rag2*^{R229Q} mice could be facilitated by the expanded lymphatic network. To test this hypothesis, allophycocyanin-labeled OVA antigen was intradermally injected in the ear pinna of mice, and its uptake and transport by DCs was evaluated in the skin and draining lymph nodes (DLNs) after 6 hours. Comparable frequencies of OVA-loaded DCs were detected locally within the skin tissue of *Rag2*^{R229Q} and *Rag2*$^{+/+}$ mice (Fig 5, *D*). However, consistent with the enhanced EB dye transport, a higher proportion of OVA-positive DCs was recovered in the DLNs of *Rag2*^{R229Q} mice compared with in controls (Fig 5, *D*).

Skin disease in *Rag2*^{R229Q} mice is exacerbated by intestinal inflammation

The aforementioned results indicate that endogenous Tlr4 ligands could have a role in cutaneous inflammation of *Rag2*^{R229Q} mice. We previously reported high levels of endotoxin (LPS) in the circulation of *Rag2*^{R229Q} mice correlating with gut dysbiosis and intestinal inflammation.[20] Increased levels of LPS-binding protein, marker of microbial load and translocation, were detected also in sera of patients with OS (Fig 6, *A*), with the highest levels found in patients exhibiting intestinal inflammation and profuse diarrhea. To evaluate whether high serum endotoxin may contribute to skin inflammation in *Rag2*^{R229Q} mice, we analyzed the cutaneous responses to systemic LPS. Mice received a single injection of 100 μg LPS intraperitoneally and were sacrificed 24 hours later. Histological examination of skin biopsies showed worsening of inflammation over baseline condition in *Rag2*^{R229Q} mice, with increased epidermal thickening, hyperkeratosis, occasional abscesses, and more prominent dermal infiltrates (Fig 6, *B* and *C*). Signs of inflammation were evident also in the skin of LPS-treated *Rag2*$^{+/+}$ mice, similar to those observed in untreated *Rag2*^{R229Q} mice (Fig 6, *C*). Furthermore, on LPS challenge, levels of *Tlr4* and *Ifng* transcripts were significantly upregulated in *Rag2*^{R229Q} mice and, to a lesser extent, in *Rag2*$^{+/+}$ mice (Fig 6, *D*), indicating that systemic endotoxin can play a role in the cutaneous inflammation of *Rag2*^{R229Q} mice. Skin homeostasis was not markedly altered in mutant mice at weaning, likely reflecting the reduced LBP levels compared with LBP levels in adult mice and the time of exposure to endotoxin (Fig E5 in this article's Online Repository at www.jacionline.org).

Moreover, we observed that *Rag2*^{R229Q} mice in which the skin inflammation was more pronounced were those in which intestinal disease was also more severe (Fig 6, *E* and *F*). To determine the potential role of the gut-skin axis in the disease pathophysiology, we boosted intestinal inflammation in *Rag2*^{R229Q} mice using chronic dextran sulfate sodium salt (DSS) treatment. Mice were sacrificed after 4 weeks. DSS-treated *Rag2*^{R229Q} mice manifested worsened skin inflammation, as indicated by enhanced epidermal thickening, hyperkeratosis, and increased number of CD3$^+$ T cells infiltrating the dermis (Fig 7, *A*). Furthermore, immunostaining for CD31 demonstrated enhanced cutaneous vascularization in DSS-treated *Rag2*^{R229Q} mice (Fig 7, *B*). By contrast, DSS treatment did not induce similar skin abnormalities in *Rag2*$^{+/+}$ mice (Fig E6, *A* and *B* in this article's Online Repository at www.jacionline.org). FACS analysis of cutaneous cell suspensions confirmed that the proportion of skin-infiltrating CD4$^+$ T cells and CD8$^+$ T cells was increased by 2- to 4-fold in DSS-treated *Rag2*^{R229Q} mice (Fig 7, *C*). Moreover, the frequency of circulating CD4$^+$ Ccr4$^+$ T cells was significantly increased in DSS-*Rag2*^{R229Q} mice (Fig 7, *F*), with a significant proportion co-expressing also the gut-homing receptor Ccr9 (Fig 7, *F*), thus suggesting that memory T cells in *Rag2*^{R229Q} mice may recirculate between skin and intestinal mucosa. Cutaneous levels of *Cxcr3* and *Ifng* transcripts were upregulated in DSS-*Rag2*^{R229Q} mice (Fig 7, *D*), leading to enhanced epithelial expression of MHC-II molecules and keratinocyte hyperactivation (Fig 7, *E*).[34]

Finally, we investigated whether the mechanism for endotoxin-driven skin disease exacerbation is applicable to mice not displaying preexisting inflammatory bowel disease. To this end, we tested the effect of acute DSS in a mouse model of AD. Experimental AD was induced by daily topical application of the vitamin D3 analog MC903 on the ears. At day 8, groups of mice received for 7 days water with or without 2% DSS, followed by normal drinking water for an additional 2 days, and then euthanized. Plasma LBP was significantly augmented in mice receiving DSS administration (Fig E7, *A* in this article's Online Repository at www.jacionline.org), which caused increased swelling, reddening, and scaling of the skin in the treated mice (Fig E7, *B* and *C*). Microscopic investigation revealed a stronger dermal inflammatory cell infiltration with epidermal hyperplasia and hyperkeratosis in DSS-treated AD mice (Fig E7, *D*). Consistent with increased inflammation, the expression of T_H1 and T_H2 inflammatory markers was augmented (Fig E7, *E*).

Collectively, these results suggest that a leaky gut plays an important role in priming the skin disease for a hyperinflammatory response to systemic LPS.

Rag2^{R229Q} (*blue dots*). The Spearman *r* value is indicated in the graph (n = 5 mice/group). **C,** Fold change of the CD4$^+$ and CD8$^+$ T-cell frequencies (n = 6-9 mice/group). **D,** Fold change of cutaneous *Cxcr3, Cxcl10, Ifng, Ccl20, Tslp,* and *Tlr4* expressions (n = 6-9 mice/group). **E,** MFI for MHCII expression among CD45$^-$ population of *Rag2*^{R229Q} and DSS-treated *Rag2*^{R229Q} skin suspension (n = 5-6 mice/group). **F,** Representative FACS plots and cumulative frequencies of splenic Ccr4$^+$, Ccr9$^+$, and Ccr4$^+$Ccr9$^+$ CD4$^+$ T cells (n = 6-11 mice/group from 3 experiments). *Dotted line* indicates WT averages. Values are mean ± SEM. **P* < .05; ***P* < .01; ****P* < .005. Statistical significance determined by Mann-Whitney *U* test. See also Fig E4.

DISCUSSION

The cutaneous hallmark of OS is a severe exfoliative erythroderma, resulting in epidermal barrier defect and subsequent risk of life-threatening bacterial infections. The aberrant expression of skin-homing molecules CLA and CCR4 on T cells from patients with OS, together with the high CCL17/CCL22 serum levels, indicates that they are poised to migrate to the inflamed skin and have pathogenic potential.[35] Along with high serum levels of IL-13 and IL-5, these observations may also sustain the notion that OS is a T_H2-driven disease. Surprisingly, we detected high levels also of IFN-γ, CXCL9, and CXCL10 in the serum of patients with OS. Similar results have been demonstrated both in the skin and in circulation of *Rag2*^{R229Q} mice, indicating that OS is not a pure T_H2-driven disease, but rather manifests a broad inflammatory signature, with a prominent role also for T_H1-mediated responses. Many studies reported promiscuous expression of chemokines in the serum of patients with cutaneous inflammation,[36] proposing that the immunological phenotype in T-cell–mediated skin diseases can shift toward a $T_H2/T_H1/T_H17$ mixed response as the duration of the disease increases.[37] Furthermore, although expression of CCR4 is more commonly associated with T_H2 responses, it has also been observed on T_H17 cells, suggesting that the chemokines activating this receptor may have a broader impact on the inflammatory response than simply recruiting T_H2 cells.[38] Indeed, CCR4$^+$ memory T cells also contain non-T_H2 populations expressing CXCR3 and IFN-γ[39] and CCL17 and CCL22 can be released not only by leukocytes, but also by activated dermal endothelial cells and keratinocytes, in response to both T_H1 and T_H2 cytokines.[34] Both CCR4 and CXCR3 antagonists are available for the treatment of allergic disease and psoriasis[40,41] and may represent a novel therapeutic target also in OS.

Increased expression of *Tlr4* and downstream signaling molecules *Myd88* and *Trif* in the skin of *Rag2*^{R229Q} mice correlated with hyperinflammatory cutaneous responses on topical or systemic administration of LPS. Together with our previous demonstration of inflammatory bowel disease–like disease, altered gut microbiota, and elevated LPS serum levels in *Rag2*^{R229Q} mice,[20] these findings suggest that endogenous Tlr4 ligands play a role in the maintenance of keratinocyte activation and perpetuation of local inflammatory response.[42] Consistently, DSS treatment markedly worsened cutaneous inflammation in *Rag2*^{R229Q} mice. Chronic gastrointestinal diseases, such as inflammatory bowel disease or celiac disease, are often associated with skin inflammation.[43,44] Likewise, marked changes in gut barrier and in intestinal microbiota are observed in AD and patients with rosacea.[45] However, it cannot be excluded that inflammation in other organs may also contribute to increase the severity of skin inflammation in OS.[46]

High cutaneous expression of antimicrobial peptides and Tlrs in the *Rag2*^{R229Q} mice is indicative of important alterations of skin barrier integrity and microbial challenge. Changes of the cutaneous microbiota have been correlated with several skin disorders.[47-49] Here we have shown that *Rag2*^{R229Q} mice manifested a selective shift in resident skin microbiota with decreased abundance of commensal bacteria belonging to Actinobacteria and Firmicutes phyla. The loss of some protective bacteria genera (*Streptococcus*, *Staphylococcus,* and *Propionibacterium*) might render the skin of *Rag2*^{R229Q} mice more susceptible to development of local inflammation. These data indicate the importance of performing similar studies also in patients with OS, although the frequent use of immunosuppressive agents and antibiotics in these patients may affect interpretation of the results.

Similar to patients with OS, an increased proportion of Ccr4-expressing CD4$^+$ T cells was detectable in lymphoid organs of *Rag2*^{R229Q} mice, indicating that these cells are poised to migrate to the skin. Interestingly, we observed coexpression of skin-homing (Ccr4) and gut-homing (Ccr9) expression by a subset of splenic T cells in DSS-treated *Rag2*^{R229Q} mice, suggesting that these cells might be potentially able to recirculate between gut and skin. Plasticity in the migratory property of immune cells has been suggested. Particularly, cutaneous exposure to food antigens can reprogram LN effector T cells expressing gut-homing receptors to express skin-homing receptors, thereby eliciting skin inflammation.[50] Tissue-derived DCs have a key role in presenting local antigens and imprinting T cells with specific homing properties. Trafficking of skin-derived DCs to DLNs is increased in *Rag2*^{R229Q} mice, correlating with abundant lymphatic network. Moreover, we previously described an augmented population of migratory CD103+ DCs in the spleen of *Rag2*^{R229Q} mice,[51] suggesting that reprogramming of T cell homing by tissue-derived DCs may also occur in secondary lymphoid organs other than DLNs. Intriguingly, skin-derived and antigen-bearing DCs were also identified in MLNs.[50] Hence, breaches of skin and gut barriers in *Rag2*^{R229Q} mice may promote systemic translocation of microbial antigens and induce activation of T cells expressing homing receptors for skin and/or gut. In summary, we have demonstrated that the cutaneous manifestations of OS are characterized by a broad inflammatory signature and can be severely influenced by gut inflammation, reinforcing the notion of an interplay between skin and gut in the pathophysiology of the disease.

Key messages

- **A broad $T_H1/T_H2/T_H17$ inflammatory signature is observed in the blood and skin of patients with OS and in the murine model.**
- **Systemic LPS injection or boosting colitis in OS murine model aggravates cutaneous T-cell infiltration and skin inflammation.**
- **High level of serum endotoxin is detected in patients with OS.**

REFERENCES

1. Nestle FO, Di Meglio P, Qin JZ, Nickoloff BJ. Skin immune sentinels in health and disease. Nat Rev Immunol 2009;9:679-91.
2. Gebhardt T, Whitney PG, Zaid A, Mackay LK, Brooks AG, Heath WR, et al. Different patterns of peripheral migration by memory CD4+ and CD8+ T cells. Nature 2011;477:216-9.
3. Bromley SK, Yan S, Tomura M, Kanagawa O, Luster AD. Recirculating memory T cells are a unique subset of CD4+ T cells with a distinct phenotype and migratory pattern. J Immunol 2013;190:970-6.
4. Berg EL, Yoshino T, Rott LS, Robinson MK, Warnock RA, Kishimoto TK, et al. The cutaneous lymphocyte antigen is a skin lymphocyte homing receptor for the vascular lectin endothelial cell-leukocyte adhesion molecule 1. J Exp Med 1991; 174:1461-6.
5. Campbell JJ, Haraldsen G, Pan J, Rottman J, Qin S, Ponath P, et al. The chemokine receptor CCR4 in vascular recognition by cutaneous but not intestinal memory T cells. Nature 1999;400:776-80.
6. Reiss Y, Proudfoot AE, Power CA, Campbell JJ, Butcher EC. CC chemokine receptor (CCR)4 and the CCR10 ligand cutaneous T cell-attracting chemokine (CTACK) in lymphocyte trafficking to inflamed skin. J Exp Med 2001;194:1541-7.

7. Homey B, Alenius H, Muller A, Soto H, Bowman EP, Yuan W, et al. CCL27-CCR10 interactions regulate T cell-mediated skin inflammation. Nat Med 2002; 8:157-65.
8. Mora JR, Von Andrian UH. Specificity and plasticity of memory lymphocyte migration. Curr Top Microbiol Immunol 2006;308:83-116.
9. Hart AL, Ng SC, Mann E, Al-Hassi HO, Bernardo D, Knight SC. Homing of immune cells: role in homeostasis and intestinal inflammation. Inflamm Bowel Dis 2010;16:1969-77.
10. Lehman H. Skin manifestations of primary immune deficiency. Clin Rev Allergy Immunol 2014;46:112-9.
11. Oh J, Freeman AF, Park M, Sokolic R, Candotti F, Holland SM, et al., for the NISC Comparative Sequencing Program. The altered landscape of the human skin microbiome in patients with primary immunodeficiencies. Genome Res 2013;23:2103-14.
12. Notarangelo LD, Kim MS, Walter JE, Lee YN. Human RAG mutations: biochemistry and clinical implications. Nat Rev Immunol 2016;16:234-46.
13. Scheimberg I, Hoeger PH, Harper JI, Lake B, Malone M. Omenn's syndrome: differential diagnosis in infants with erythroderma and immunodeficiency. Pediatr Dev Pathol 2001;4:237-45.
14. Maina V, Marrella V, Mantero S, Cassani B, Fontana E, Anselmo A, et al. Hypomorphic mutation in the RAG2 gene affects dendritic cell distribution and migration. J Leukoc Biol 2013;94:1221-30.
15. Smith PD, MacDonald TT, Blumberg RS, Society for Mucosal Immunology. Principles of mucosal immunology. London: Garland Science/Taylor & Francis Group; 2013.
16. Parodi A, Paolino S, Greco A, Drago F, Mansi C, Rebora A, et al. Small intestinal bacterial overgrowth in rosacea: clinical effectiveness of its eradication. Clin Gastroenterol Hepatol 2008;6:759-64.
17. Wang M, Karlsson C, Olsson C, Adlerberth I, Wold AE, Strachan DP, et al. Reduced diversity in the early fecal microbiota of infants with atopic eczema. J Allergy Clin Immunol 2008;121:129-34.
18. Forno E, Onderdonk AB, McCracken J, Litonjua AA, Laskey D, Delaney ML, et al. Diversity of the gut microbiota and eczema in early life. Clin Mol Allergy 2008;6:11.
19. Zanvit P, Konkel JE, Jiao X, Kasagi S, Zhang D, Wu R, et al. Antibiotics in neonatal life increase murine susceptibility to experimental psoriasis. Nat Commun 2015;6:8424.
20. Rigoni R, Fontana E, Guglielmetti S, Fosso B, D'Erchia AM, Maina V, et al. Intestinal microbiota sustains inflammation and autoimmunity induced by hypomorphic RAG defects. J Exp Med 2016;213:355-75.
21. Fuhlbrigge RC, Kieffer JD, Armerding D, Kupper TS. Cutaneous lymphocyte antigen is a specialized form of PSGL-1 expressed on skin-homing T cells. Nature 1997;389:978-81.
22. Biedermann T, Schwarzler C, Lametschwandtner G, Thoma G, Carballido-Perrig N, Kund J, et al. Targeting CLA/E-selectin interactions prevents CCR4-mediated recruitment of human Th2 memory cells to human skin in vivo. Eur J Immunol 2002;32:3171-80.
23. Marrella V, Poliani PL, Casati A, Rucci F, Frascoli L, Gougeon ML, et al. A hypomorphic R229Q Rag2 mouse mutant recapitulates human Omenn syndrome. J Clin Invest 2007;117:1260-9.
24. de Guzman Strong C, Wertz PW, Wang C, Yang F, Meltzer PS, Andl T, et al. Lipid defect underlies selective skin barrier impairment of an epidermal-specific deletion of Gata-3. J Cell Biol 2006;175:661-70.
25. Aberg KM, Man MQ, Gallo RL, Ganz T, Crumrine D, Brown BE, et al. Co-regulation and interdependence of the mammalian epidermal permeability and antimicrobial barriers. J Invest Dermatol 2008;128:917-25.
26. Schwarz A, Bruhs A, Schwarz T. The short-chain fatty acid sodium butyrate functions as a regulator of the skin immune system. J Invest Dermatol 2017;137: 855-64.
27. Komine M, Rao LS, Freedberg IM, Simon M, Milisavljevic V, Blumenberg M. Interleukin-1 induces transcription of keratin K6 in human epidermal keratinocytes. J Invest Dermatol 2001;116:330-8.
28. Nestle FO, Turka LA, Nickoloff BJ. Characterization of dermal dendritic cells in psoriasis: autostimulation of T lymphocytes and induction of Th1 type cytokines. J Clin Invest 1994;94:202-9.
29. Pasparakis M, Haase I, Nestle FO. Mechanisms regulating skin immunity and inflammation. Nat Rev Immunol 2014;14:289-301.
30. Elias PM. The skin barrier as an innate immune element. Semin Immunopathol 2007;29:3-14.
31. Zhang LJ. Type 1 interferons potential initiating factors linking skin wounds with psoriasis pathogenesis. Front Immunol 2019;10:1440.
32. Randolph GJ, Ivanov S, Zinselmeyer BH, Scallan JP. The lymphatic system: integral roles in immunity. Annu Rev Immunol 2017;35:31-52.
33. Liao S, Ruddle NH. Synchrony of high endothelial venules and lymphatic vessels revealed by immunization. J Immunol 2006;177:3369-79.
34. Albanesi C, Scarponi C, Sebastiani S, Cavani A, Federici M, Sozzani S, et al. A cytokine-to-chemokine axis between T lymphocytes and keratinocytes can favor Th1 cell accumulation in chronic inflammatory skin diseases. J Leukoc Biol 2001;70:617-23.
35. Fierro MT, Comessatti A, Quaglino P, Ortoncelli M, Osella Abate S, Ponti R, et al. Expression pattern of chemokine receptors and chemokine release in inflammatory erythroderma and Sezary syndrome. Dermatology 2006;213:284-92.
36. Lonsdorf AS, Hwang ST, Enk AH. Chemokine receptors in T-cell-mediated diseases of the skin. J Invest Dermatol 2009;129:2552-66.
37. Di Cesare A, Di Meglio P, Nestle FO. A role for Th17 cells in the immunopathogenesis of atopic dermatitis? J Invest Dermatol 2008;128:2569-71.
38. Lim HW, Lee J, Hillsamer P, Kim CH. Human Th17 cells share major trafficking receptors with both polarized effector T cells and FOXP3+ regulatory T cells. J Immunol 2008;180:122-9.
39. Andrew DP, Ruffing N, Kim CH, Miao W, Heath H, Li Y, et al. C-C chemokine receptor 4 expression defines a major subset of circulating nonintestinal memory T cells of both Th1 and Th2 potential. J Immunol 2001;166:103-11.
40. Charo IF, Ransohoff RM. The many roles of chemokines and chemokine receptors in inflammation. New Engl J Med 2006;354:610-21.
41. Subramaniam JM, Whiteside G, McKeage K, Croxtall JC. Mogamulizumab: first global approval. Drugs 2012;72:1293-8.
42. Song PI, Park YM, Abraham T, Harten B, Zivony A, Neparidze N, et al. Human keratinocytes express functional CD14 and Toll-like receptor 4. J Invest Dermatol 2002;119:424-32.
43. Huang BL, Chandra S, Shih DQ. Skin manifestations of inflammatory bowel disease. Front Physiol 2012;3:13.
44. Leffler DA, Green PH, Fasano A. Extraintestinal manifestations of coeliac disease. Nat Rev Gastroenterol Hepatol 2015;12:561-71.
45. Weinstock LB, Steinhoff M. Rosacea and small intestinal bacterial overgrowth: prevalence and response to rifaximin. J Am Acad Dermatol 2013;68:875-6.
46. Orange JS. Congenital immunodeficiencies and sepsis. Pediatr Crit Care Med 2005;6(3 Suppl):S99-107.
47. Naik S, Bouladoux N, Wilhelm C, Molloy MJ, Salcedo R, Kastenmuller W, et al. Compartmentalized control of skin immunity by resident commensals. Science 2012;337:1115-9.
48. Gao Z, Tseng CH, Strober BE, Pei Z, Blaser MJ. Substantial alterations of the cutaneous bacterial biota in psoriatic lesions. PLoS One 2008;3:e2719.
49. Kong HH, Oh J, Deming C, Conlan S, Grice EA, Beatson MA, et al. Temporal shifts in the skin microbiome associated with disease flares and treatment in children with atopic dermatitis. Genome Res 2012;22: 850-9.
50. Oyoshi MK, Elkhal A, Scott JE, Wurbel MA, Hornick JL, Campbell JJ, et al. Epicutaneous challenge of orally immunized mice redirects antigen-specific gut-homing T cells to the skin. J Clin Invest 2011;121: 2210-20.
51. Rigoni R, Grassi F, Villa A, Cassani B. RAGs and BUGS: an alliance for autoimmunity. Gut Microbes 2016;7:503-11.

METHODS

Histology and immunohistochemistry

Mouse tissue samples were formalin-fixed and paraffin-embedded. Sections (1.5 μm) were used for routine H&E staining. Moreover, sections were dewaxed and rehydrated; endogenous peroxidase activity was blocked by 0.1% H_2O_2; nonspecific background was reduced with Rodent Block (Biocare Medical, Pacheco, Calif) before microwaves or thermostatic bath treatment; and incubated with primary antibodies. The following primary antibodies were used: rabbit anti-CD3 (1:100; EDTA buffer pH 8.0; 1 hour at room temperature [RT]; Thermo Fisher Scientific), rabbit anti-Ki67 (1:350; citrate buffer pH 6.0; 1 hour RT; Cell Signaling Technology, Danvers, Mass), rabbit anti-keratin 5 (1:200; EDTA buffer pH 8.0; 1 hour RT; BioLegend), rabbit anti-myeloperoxidase (1:300; EDTA buffer pH 8.0; overnight; Abcam, Cambridge, Mass), and goat anti-CD31 (1:1000; R&D Systems; DIVA Decloaker 1×; Biocare Medical). Depending on the primary antibodies and tissue used, sections were incubated with Goat-on-Mouse HRP-Polymer (Biocare Medical), MACH 1 Universal HRP Polymer Kit (Biocare Medical); reactions were developed in Biocare's Betazoid DAB; and nuclei were counterstained with Hematoxylin (Dako, Agilent, Santa Clara, Calif). Digital images were acquired by an Olympus XC50 camera mounted on a BX51 microscope (Olympus, Tokyo, Japan) or by an Olympus DP70 camera mounted on a BX60 microscope (Olympus), with CellF Imaging software (Soft Imaging System GmbH, Münster, Germany).

Histological score. Arbitrary gut and skin histological score was calculated in a double-blind study by a pathologist. Scoring from 0 to 3 (where 0 is normal condition and 3 is severe structural changes) was adopted for evaluating different manifestations in each tissue. For gut analysis, a combined score—grade of inflammation, the structural changes of the glands, and the goblet cell depletion—was used. For skin analysis, abnormalities of keratinocytes, increased immune cells in the dermis, alterations of the epidermis, and presence of cutaneous abscesses were evaluated. Specifically, for DSS treatment, the number of $CD3^+$ aggregates was also analyzed.

Morphometric analysis. Histological dermal thickness was determined, on H&E-stained sections, by measuring the distance between the epidermal-dermal junction and dermal–subcutaneous fat junction (60 fields for each sample). Morphometric analysis to evaluate coverage, number of vessels, and size was determined on CD31-stained sections. Both analyses were performed using Olympus Slide Scanner VS120-L100 to acquire digital images and Image-Pro software (Media Cybernetics, Rockville, Md).

Mice and *in vivo* treatments

OT-I and OT-II adoptive transfer. Splenic $CD8^+$ OT-I cells or $CD4^+$ OT-II cells were sorted from donor mice. T cells (3×10^6) were adoptively transferred intravenously into $Rag2^{+/+}$ and $Rag2^{R229Q}$ mice (CD45.1). The day after, ears were immunized.[E1] Briefly, both sides of each ear were gently stripped 10 times with Scotch Tape (3M, St Paul, Minn) and 25 μL of acetone was applied and evaporated. Then, 20 μL of cholera toxin (CT) or CT+ 50 μL of OVA (100 mg/mL; Sigma-Aldrich) was applied with a small paintbrush on the ears of recipient mice. $Rag2^{+/+}$ and $Rag2^{R229Q}$ mice were sacrificed after 7 days from topical immunization.

Coculture DC-T cells. Topical immunization of ear skin of $Rag2^{+/+}$ and $Rag2^{R229Q}$ mice was performed as described above. Briefly, CT plus OVA or CT alone was applied directly on ear skin. After 4 days, DCs from spleen and DLNs were sorted from OVA-immunized $Rag2^{+/+}$ and $Rag2^{R229Q}$ mice and CT controls. DCs were put in coculture with $CD4^+$ OT-II cells in 96-well round-bottom plates. A 1:1 DC–T cell ratio was used for the assay. Cocultures were maintained for 6 days and T-cell proliferation was evaluated by overnight incorporation of (3H)-thymidine.

***In vivo* treatments.** Acute DSS treatment was induced by adding 2.5% of DSS (MP Biomedicals, Santa Ana, Calif) to drinking water *ad libitum* for 6 days. Treated and untreated mice were sacrificed at day 7, and transcriptional analyses were performed on skin tissue. Chronic colitis was induced by adding 1.5% of DSS to drinking water *ad libitum* for 4 cycles for a total of 4 weeks. Control mice received water continuously throughout all the experiment. For topical and systemic LPS administration, mice were anesthetized and injected intradermally into the back with 100 μg of LPS (right side) and PBS (left side) using Hamilton syringes. After 24 hours, LPS-treated mice were sacrificed and skin tissues were processed for histological analysis and quantitative RT-PCR analysis. For systemic LPS administration, mice were injected intraperitoneally with 100 μg of LPS. Systemic LPS-treated mice were sacrificed 24 hours later. Skin tissues were used for histological scores and transcriptional analysis. Mice were injected intradermally into the ear's skin with 100 μg/mL OVA–Alexa Fluor (Thermo Fisher Scientific) with Hamilton syringe. After 6 hours, DLNs and ear tissues were collected. The analysis of OVA-loaded $CD11C^+$ DCs from ears and DLNs was performed by FACS.

***In situ* RNA hybridization.** Slides were deparaffinized in xylene (2×, 5 minutes each) and 100% ethyl alcohol (2×, 1 minute each) and air dried at RT, followed by H_2O_2 (Cat no 322330; ACDBio, Advanced Cell Diagnostics) at RT for 10 minutes. Slides were submerged in 700 mL fresh 1X Target Retrieval (Cat no 322000; ACDBio) at boiling for 15 minutes and immediately washed in deionized water followed by 100% ethyl alcohol and air dried. A hydrophobic barrier was drawn around tissue and protease plus (Cat no 322330; ACDBio) was applied for 15 minutes in a HybEZ oven (Cat no 322310; ACDBio) at 40°C. Slides were washed in deionized water and probes were added for 2 hours in the HybEZ oven. Signal amplification reagents antimicrobial peptide (AMP) 1 (30 minutes), AMP 2 (15 minutes), AMP 3 (30 minutes), AMP 4 (15 minutes), AMP 5 (75 minutes), and AMP 6 (15 minutes) were applied sequentially and incubated in the HybEZ oven. Before adding each AMP reagent, samples were washed twice with washing buffer (Cat no 310091; ACDBio). Diaminobenzidine chromogen detection reagent was applied and incubated for 10 minutes in the HybEZ oven. Samples were then counterstained, rinsed with tap water, and placed in 0.02% ammonia water followed by another tap water rinse. Samples were then dehydrated in graded alcohols followed by xylene treatment (2×, 5 minutes each) and cover slipped.

Cutaneous microbiota analysis. Weaned $Rag2^{+/+}$ and $Rag2^{R229Q}$ littermates were maintained in the separated cages until analysis. Cutaneous tissues were weighed and digested in lysis buffer (10 mmol/L TRIS, 100 mmol/L NaCl, 10 mmol/L EDTA, 0.5% SDS, and 0.4 mg/mL proteinase K). Total DNA was extracted with the isopropanol-ethanol method. Bacterial DNA was analyzed by real-time PCR using specific primers for 16s ribosomal RNA (rRNA) gene. Microbiota taxonomic profiling was carried out at GenProbio Srl (Parma, Italy). In brief, primer pairs Probio Uni and Probio_Rev[E2] (GenProbio Srl) were used for the amplification of the region 16S rRNA gene encompassing the V3 variable region; amplicons were then processed and sequenced using an Illumina MiSeq sequencer (Illumina Inc, San Diego, Calif) with MiSeq Reagent Kit chemicals (Illumina). For taxonomic classification of taxonomic units, the resulting fastq files were then processed with the bioinformatic pipeline Quantitative Insights Into Microbial Ecology ([QIIME], version 1.7.0)[E3] with the 16S rRNA gene database SILVA (version 128[E4]). To identify specific bacterial taxa distinguishing the skin microbiota of $Rag2^{+/+}$ from $Rag2^{R229Q}$ mice, we used the linear discriminant analysis effect size method.[E5] Specifically, linear discriminant analysis effect size analysis included Kruskal-Wallis and pairwise Wilcoxon tests considering significant a corrected P value of <.05.[E5]

Experimental model of AD

The induction of MC903 dermatitis was performed as previously described (6). Briefly, MC903 was applied to both ears from days 0 to 8, select cages were placed on 2% DSS water on days 8 to 15, and then all cages returned to normal drinking water for days 16 and 17. Ear thickness was measured as described on days 0, 8, and 17. On day 17, mice were euthanized, and ears and serum were harvested for further analysis.

REFERENCES

E1. Nizza ST, Campbell JJ. CD11b+ migratory dendritic cells mediate CD8 T cell cross-priming and cutaneous imprinting after topical immunization. PLoS One 2014;9e91054.

E2. Milani C, Hevia A, Foroni E, Duranti S, Turroni F, Lugli GA, et al. Assessing the fecal microbiota: an optimized ion torrent 16S rRNA gene-based analysis protocol. PLoS One 2013;8:e68739.

E3. Caporaso JG, Kuczynski J, Stombaugh J, Bittinger K, Bushman FD, Costello EK, et al. QIIME allows analysis of high-throughput community sequencing data. Nat Methods 2010;7:335-6.

E4. Quast C, Pruesse E, Yilmaz P, Gerken J, Schweer T, Yarza P, et al. The SILVA ribosomal RNA gene database project: improved data processing and web-based tools. Nucleic Acids Res 2013;41:D590-6.

E5. Segata N, Izard J, Waldron L, Gevers D, Miropolsky L, Garrett WS, et al. Metagenomic biomarker discovery and explanation. Genome Biol 2011;12:R60.

E6. Myles IA, Williams KW, Reckhow JD, Jammeh ML, Pincus NB, Sastalla I, et al. Transplantation of human skin microbiota in models of atopic dermatitis. JCI Insight 2016;1:e86955.

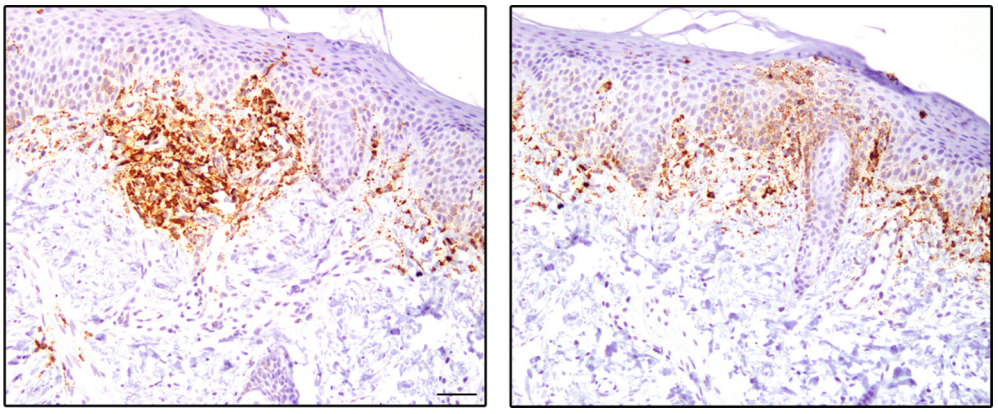

FIG E1. Elevated CXCL9 expression in skin biopsies from patients with OS. Skin biopsies from 2 patients with OS were analyzed for CXCL9 mRNA expression using RNAscope. POLR2A mRNA labeling was used as control for the quality of the RNA on paraffin section.

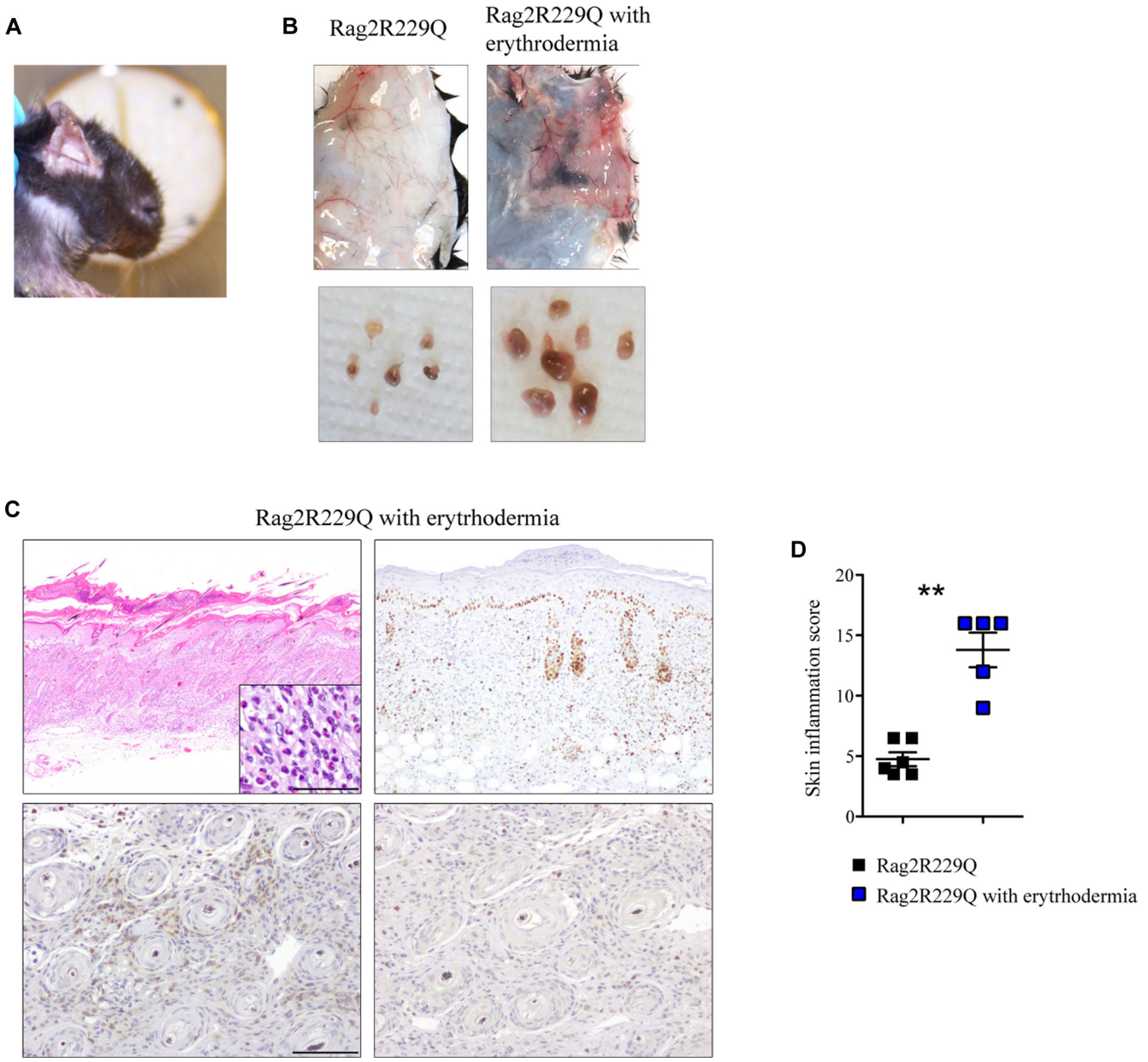

FIG E2. A small proportion of *Rag2*^{R229Q} mice exhibits erythroderma-like phenotype. **A,** Cutaneous phenotype of *Rag2*^{R229Q} mice affected by erythroderma. **B,** Macroscopic appearance of dorsal skin and lymph nodes of *Rag2*^{R229Q} and *Rag2*^{R229Q} with erythroderma-like phenotype. **C,** Representative skin sections from *Rag2*^{R229Q} with evident skin erythroderma-like phenotype stained with H&E, KI67 (*upper right*; bar = 500 μm), CD3 (*bottom left*), and myeloperoxidase (*bottom right;* bar = 100 μm) immunostaining. Higher magnification shows eosinophils. **D,** Histogram shows the inflammation score of the skin (n = 5-6 mice/group). Values are mean ± SEM. $^{**}P < .01$. Statistical analysis was performed using Mann-Whitney *U* test.

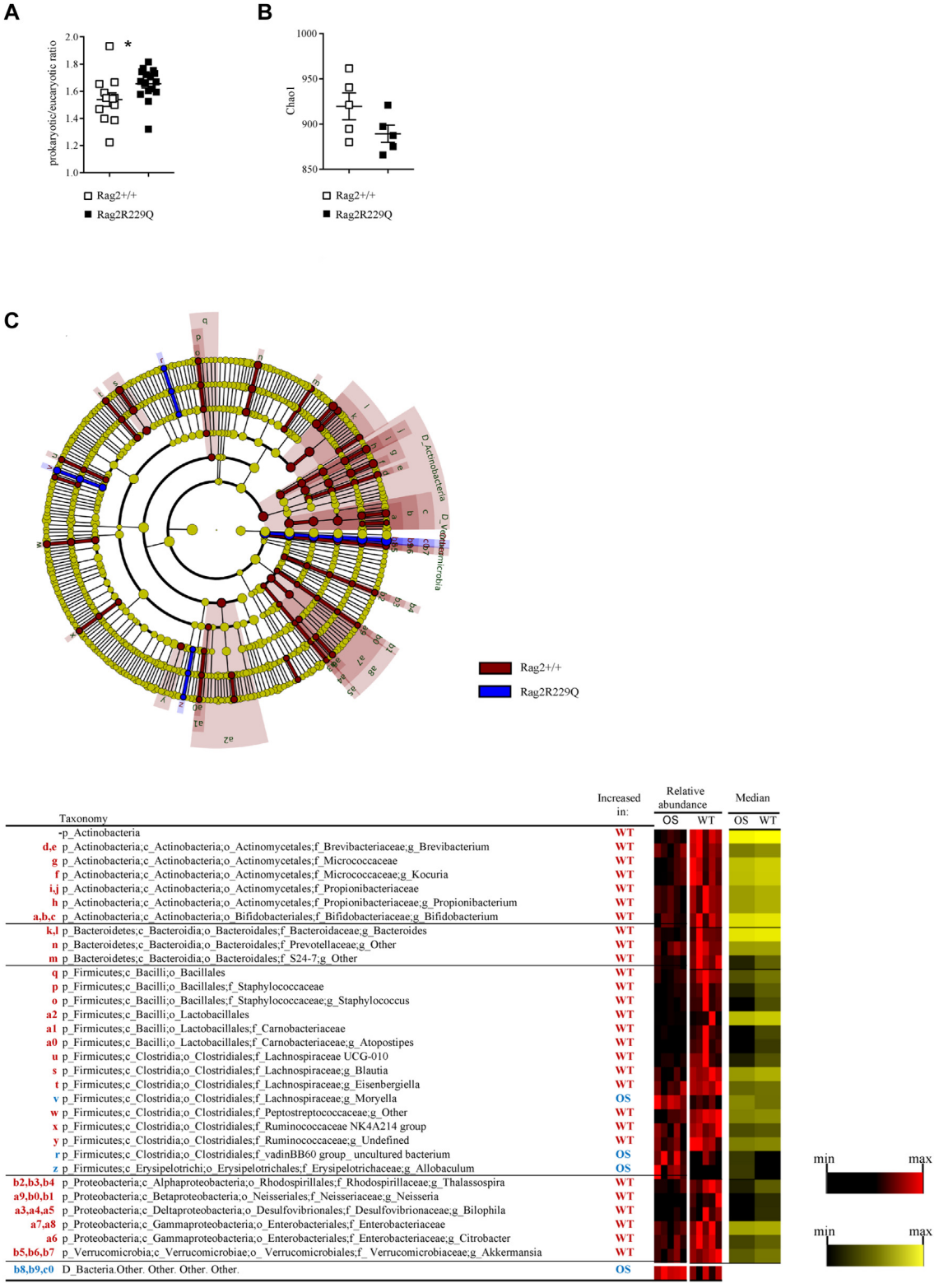

FIG E3. The composition of skin microbiota differs between *Rag2*$^{+/+}$ and *Rag2*^{R229Q} mice. Skin tissue microbiota from adults *Rag2*$^{+/+}$ (n = 10) and *Rag2*^{R229Q} (n = 10) littermates was analyzed through 16s rRNA gene profiling. **A,** Quantitative PCR analysis of cutaneous adherent bacteria in *Rag2*$^{+/+}$ and *Rag2*^{R229Q} mice expressed as prokaryotic/eukaryotic DNA (ie, 16S/18S rRNA genes) ratios (n = 12 mice/group from 3 experiments). **B,** Scatter dot plot depicts the intrasample (α) diversity (Chao1 index) describing taxonomic richness of skin microbiota in *Rag2*$^{+/+}$ and *Rag2*^{R229Q} mice. **C,** A linear discriminant analysis effect size identifies the significant different abundance of bacterial taxa between *Rag2*^{R229Q} mice and controls. The taxa with significantly different abundances among the genotypes are represented by colored shadows in the cladogram of the *top panel* and listed in the table *below*. From the center of the cladogram outward, kingdom, phylum, class, order, family, and genus levels are shown. Heat maps represent the relative abundance of significantly different taxa per sample (*black-red* heat map). Statistical analysis of data **(A, C)** was performed using Mann-Whitney *U* test. **P* < .05.

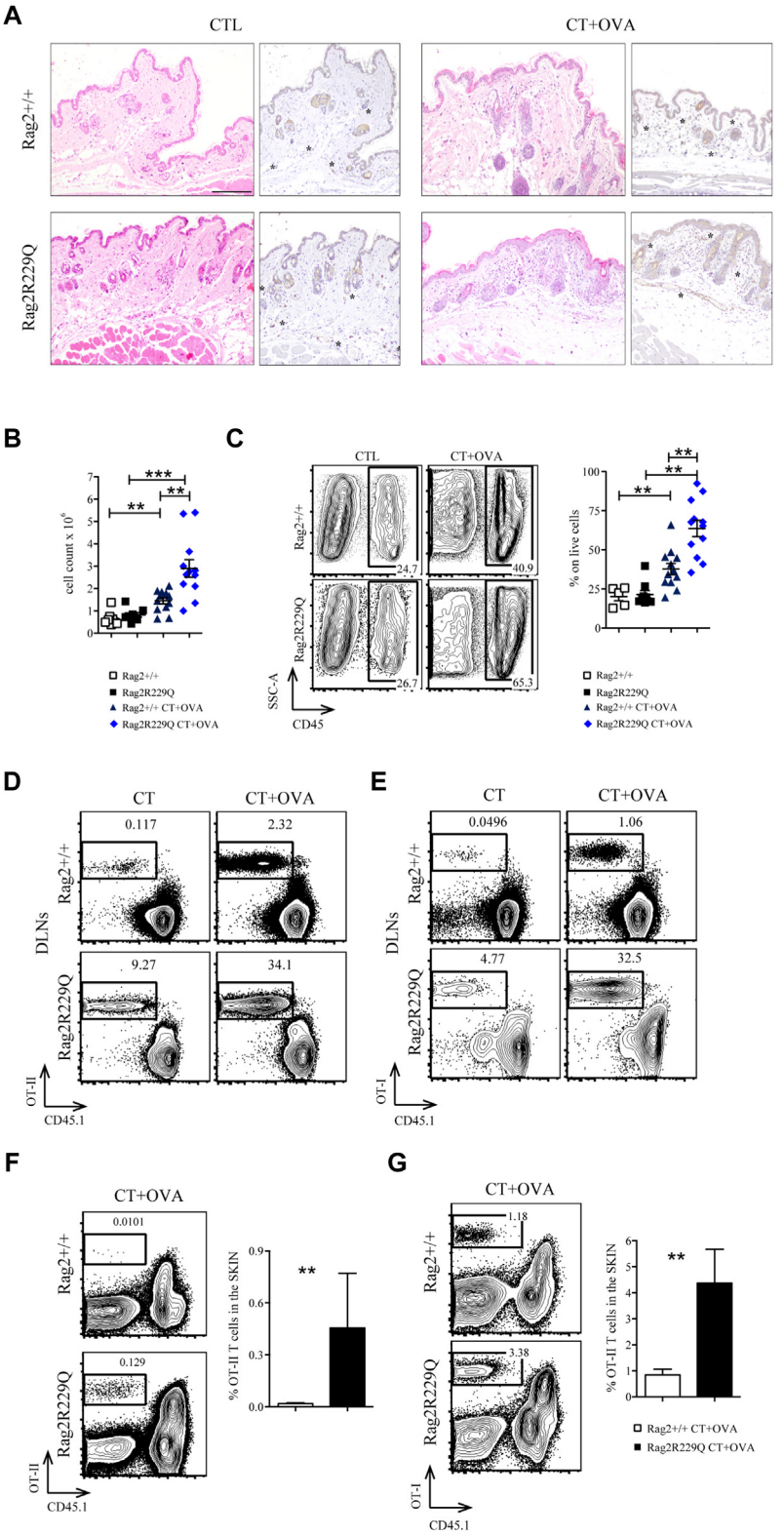

FIG E4. Cutaneous inflammatory environment in mutant mice promote T-cell infiltration. **A,** Representative skin section from controls and CT+OVA-treated *Rag2*$^{+/+}$ and *Rag2*^{R229Q} mice stained with H&E and CD31 immunostaining (*asterisks* mark the CD31-positive vessels). Bar = 200 μm. **B,** Total skin counts from skin suspension (n = 5-12). **C,** Representative FACS plot and frequencies of CD45^{+} cell population of skin suspension (n = 5-12). **D and E,** CD4 or CD8 splenocytes from OT-II or OT-I mice were adoptively transferred into *Rag2*$^{+/+}$ and *Rag2*^{R229Q} recipients. Topical immunization was applied on ears once with OVA plus CT or only CT. Recipient mice were sacrificed after 7 days. Representative dot plots of donor-derived OT-II or OT-I cells within total live population of DLN suspension. **F and G,** Representative dot plots and frequencies of donor-derived OT-II or OT-I cells within total live population of skin suspension (n = 5-7 mice/group). Values are mean ± SEM. $^{**}P < .01$; $^{***}P < .001$. Statistical analysis was performed using Mann-Whitney *U* test.

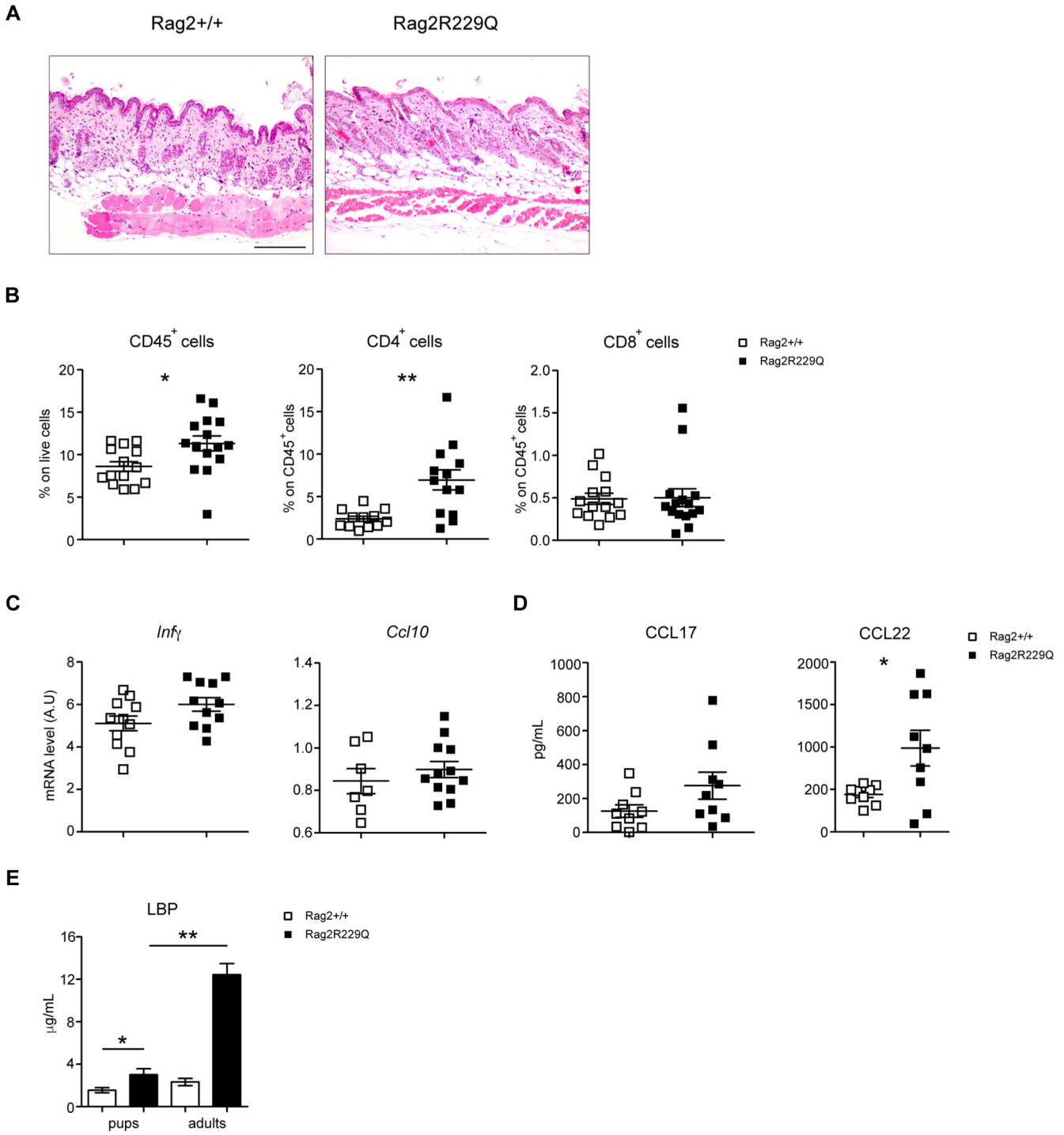

FIG E5. Analysis of skin homeostasis in young *Rag2*^{R229Q} mice. **A,** Representative skin section from 20-days-old *Rag2*$^{+/+}$ and *Rag2*^{R229Q} mice stained with H&E. Bar = 200 μm. **B,** Cumulative frequencies of CD45^{+}, CD4^{+}, and CD8^{+} T cells infiltrating the skin. **C,** Gene expression analysis of *Ifng* and *Cxcl10* in the skin tissue of *Rag2*$^{+/+}$ and *Rag2*^{R229Q} mice (n = 6-9 mice/group). Target mRNA was normalized to *Actb* mRNA. RNA contents are shown as AUs. Plasma levels of (**D**) CCL17 and CCL22 and (**E**) LPS-binding protein (*LBP*). Values are mean ± SEM. **P* < .05; ***P* < .01. Statistical analysis was performed using Mann-Whitney *U* test.

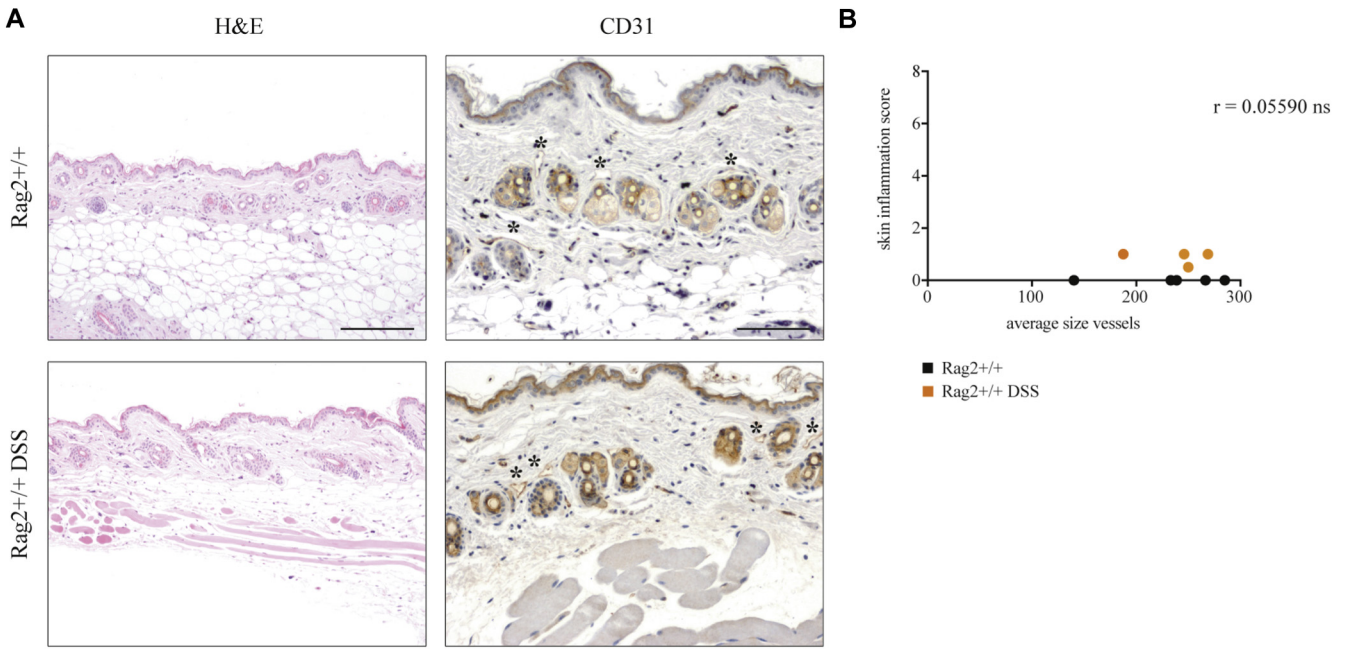

FIG E6. Cutaneous response to DSS treatment in *Rag2*$^{+/+}$ mice. **A,** Representative skin sections from untreated and DSS-treated *Rag2*$^{+/+}$ mice stained with CD31 immunostaining (*asterisks* mark the CD31-positive vessels). Bars = 100 μm. **B,** Correlation between cutaneous inflammation and average vessels size of untreated *Rag2*$^{+/+}$ (*black dots*) and DSS-treated *Rag2*$^{+/+}$ (*blue dots*). The Spearman *r* value is indicated in the graph (n = 5 mice/group).

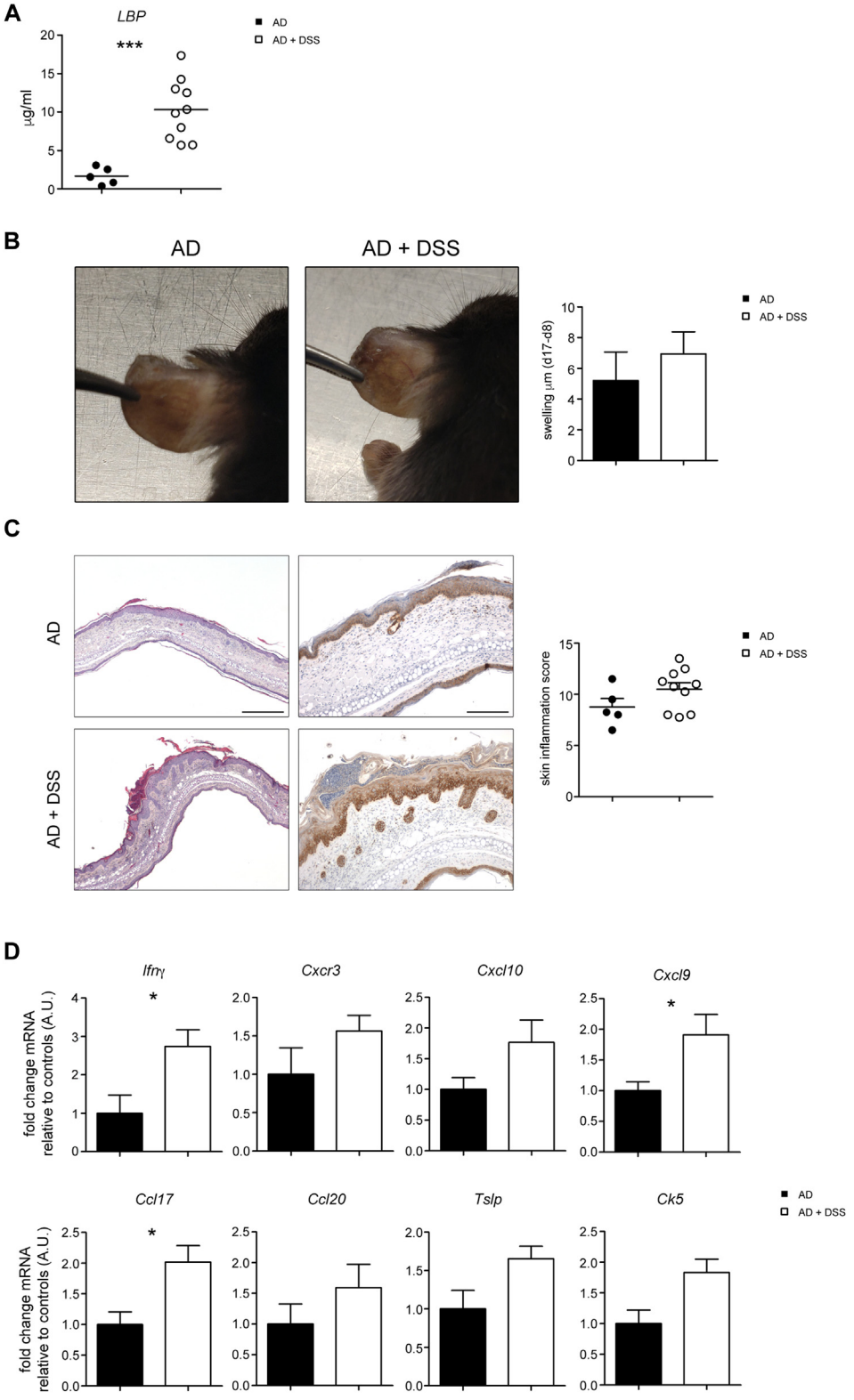

FIG E7. Effect of DSS-induced intestinal inflammation on experimental model of AD. Mice were treated with MC903 for 8 days to induce AD-like dermatitis. Starting on day 8, a set of mice received 2% DSS water for 7 days, and then returned to normal drinking water for additional 2 days. **A,** Plasma LBP on day 17 is shown. **B,** Day 17 gross phenotype of AD mice treated or not with oral DSS. Bar graph shows the difference in ear thickness between day 17 and day 8 (n = 5-10 mice/group). **C,** Representative ear section from AD and AD+DSS mice stained with H&E (*left*; bar = 500 μm) and CK5 immunostaining (*right*; bar = 200 μm). Histogram shows the inflammation score in the ear skin (n = 5-10). **D,** Gene expression analysis of the ear tissue (n = 5-10 mice/group). Target mRNA was normalized to *Actb* mRNA. RNA contents are shown as AUs. Values are mean ± SEM. **P* < .05. Statistical analysis was performed using Mann-Whitney *U* test.

TABLE E1. Clinical features of *RAG* patients

ID patient	Gene	Mutation	Erythroderma	Colitis/diarrhea	Autoimmunity	Diagnosis
SCID-400-MX	*RAG2*	p. [L155P; R229W]	Yes	Yes	No	OS
SCID-417-UK	*RAG1*	p. [R410Q/M1006V; M435V/M1006V]	Yes	No	No	OS
SCID-418-UK	*RAG1*	p.[R396C; R404Q]	Yes	Yes	No	OS
SCID-419-UK	*RAG1*	p. [R561C; R716W]	Yes	Yes	No	OS
SCID-420-UK	*RAG1*	p.[M435V/R897*; M1006V]	Yes	Infectious (rotavirus)	No	OS
SCID-421-UK	*RAG1*	p.[K86Vfs*33; R559S]	Yes	Infectious (enterovirus)	ITP, hepatitis	OS
SCID-426-KW	*RAG1*	p. [L454Q; L454Q]	Yes	No	No	OS
SCID-454-IT	*RAG1*	p. [E147fs*27; E147fs*27]	Yes	Yes	No	OS
731-UK	*RAG1*	p. [R829fs*2; K86Vfs*33]	Yes	Yes	No	OS
769-AF	*RAG1*	p. [K186Sfs*15; K186Sfs*15]	Yes	Yes	No	OS
884-PA	*RAG1*	p. [Q242R/R404Q; N766I]	Yes	Yes	No	OS
SCID-375-MX	*RAG2*	p. [G35V; G35V]	Yes	Yes	No	OS
SCID-452-KW	*RAG1*	p. [R394W; R394W]	Yes	Yes	No	OS
HIE-118-LB	*RAG1*	p. [R404W; R737H]	Yes	No	ITP, AIHA	OS

AIHA, Autoimmune hemolytic anemia; *ITP*, idiopathic thrombocytopenic purpura; *SCID*, severe combined immunodeficiency.

TABLE E2. List of primers used in this study

Primer ID	5′-3′ Sequence
Actb For	CTAAGGCCAACCGTGAAAAG
Actb Rev	ACCAGAGGCATACAGGGACA
IL-17A For	TCCAGAAGGCCCTCAGACTA
IL-17A Rev	TGAGCTTCCCAGATCACAGA
IFN-γ For	TCAAGTGGCATAGATGTGGAAGAA
IFN-γ Rev	TGGCTCTGCAGGATTTTCATG
IL-5 For	ATCCAGGAACTGCCTCGTC
IL-5 Rev	ATCCAGGAACTGCCTCGTC
IL-13 For	CCTCTGACCCTTAAGGAGCTTAT
IL-13 Rev	CGTTGCACAGGGGAGTCT
IL-33 For	TCCTTGCTTGGCAGT
IL-33 Rev	TGCTCAATGTGTCAA
TNF-α For	GACGTGGAACTGGCAGAAGAG
TNF-α Rev	TTGGTGGTTTGTGAGTGTGAG
IL-1β For	GCCCATCCTCTGTGACTCAT
IL-1β Rev	AGGCCACAGGTATTTTGTCG
CCL20 For	AACTGGGTGAAAAGGGCTGT
CCL20 Rev	GTCCAATTCCATCCCAAAAA
CXCL10 For	GCTGCCGTCATTTTCTGC
CXCL10 Rev	TCTCACTGGCCCGTCATC
CXCL9 For	CTTTTCCTCTTGGGCATCAT
CXCL9 Rev	GCATCGTGCATTCCTTATCA
16s For	GTGSTGCAYGGYTGTCGTCA
16s Rev	ACGTCRTCCMCACCTTCCTC
18s For	CTCAACACGGGAAACCTCCTCAC
18s Rev	CGCTCCACCAACTAAGAAGG
IL-23p19 For	AGCCAGTTCTGCTTGCAAAGG
IL-23p19 Rev	GGAGGTTGTGAAGTTGCTCCATG
Cramp For	AAGGAGACTGTATGTGGCAAGGCA
Cramp Rev	TTTCTTGAACCGAAAGGGCTGTGC
mBD-3 For	GTCAGATTGGCAGTTGTGGA
mBD-3 Rev	GCTAGGGAGCACTTGTTTGC
VEGF-A For	CAGGGCTTCATCGTTACAG
VEGF-A Rev	CATCTTCAAGCCGTCCTGT
TLR-2 For	AGCATCCTCTGAGATTTGA
TLR-2 Rev	GGGGCTTCACTTCTCTGCTT
TLR-3 For	TCCCCCAAAGGAGTACATT
TLR-3 Rev	GATACAGGGATTGCACCCA
TLR-4 For	GGACTCTGATCATGGCACTG
TLR-4 Rev	CTGATCCATGCATTGGTAGGT
TLR-5 For	CTGGAGCCGAGTGAGGTC
TLR-5 Rev	CGGCAAGCATTGTTCTCC
TLR-9 For	GAGAATCCTCCATCTCCCAAC
TLR-9 Rev	CCAGAGTCTCAGCCAGCAC
TSLP For	CAGCTTCGTCTCCTGA
TSLP Rev	AAATGTTTTGTCGGGGAGTG
CK5 For	CATTCTCAGCCGTGGTACG
CK5 Rev	CAGAGCTGAGGAACATGCAG
CK6 For	GTCCAGGACCTTGTTCTGCT
CK6 Rev	ATCCAGCGGGTCAGGACT
CCL22 For	CTGATGCAGGTCCTATGGT
CCL22 Rev	GGAGTAGCTTCTTCACCCAG
CCL17 Rev	TGCTTCTGGGGACTTTTCTG
CCL17 For	GAATGGCCCCTTTGAAGTAA
CXCR3 Rev	GGCATCTAGCACTTGACGTTC
CXCR3 For	GCAGCACGAGACCTGACC
Loricrin Rev	CATGAGAAAGTTAAGCCCATG
Loricrin For	GGTTGCAACGGAGACAACA
Involucrin Rev	TTGAGAGGTCCCTGAACCAC
Involucrin For	TCCTGTGAGTTTGTTTGGTC

For, Forward; *Rev*, reverse.